Gondwana Research 82 (2020) 128–150

Contents lists available at ScienceDirect

Gondwana Research

journal homepage: www.elsevier.com/locate/gr

Geochemistry, geochronology and petrogenesis of Maya Block granitoids and dykes from the Chicxulub Impact Crater, Gulf of México: Implications for the assembly of Pangea

Jiawei Zhao [a], Long Xiao [a,b,*], Sean P.S. Gulick [c], Joanna V. Morgan [d], David Kring [e], Jaime Urrutia Fucugauchi [f], Martin Schmieder [e], Sietze J. de Graaff [g], Axel Wittmann [h], Catherine H. Ross [c], Philippe Claeys [g], Annemarie Pickersgill [i,r], Pim Kaskes [g], Steven Goderis [g], Cornelia Rasmussen [j], Vivi Vajda [k], Ludovic Ferrière [l,m], Jean–Guillaume Feignon [m], Elise Chenot [n], Ligia Perez-Cruz [o], Honami Sato [p], Kosei Yamaguchi [q], IODP–ICDP Expedition 364 scientists

[a] State Key Laboratory of Geological Processes and Mineral Resources, Planetary Science Institute, School of Earth Sciences, China University of Geosciences, Wuhan, China
[b] State Key Laboratory of Space Science Institute, Lunar and Planetary Science, Macau university of Science and Technology, Taipa, Macau, China
[c] Institute for Geophysics, Jackson School of Geosciences, University of Texas at Austin, TX 78758-4445, USA
[d] Department of Earth Science and Engineering, Imperial College London, London SW7 2BP, UK
[e] Lunar and Planetary Institute, 3600 Bay Area Boulevard, Houston, TX 77058, USA
[f] Instituto de Geofisica, Universidad Nacional Autónoma de México, México D.F., México
[g] Analytical, Environmental and Geo–Chemistry, Vrije Universiteit Brussel, Pleinlaan 2, 1050 Elsene, Belgium
[h] Eyring Materials Center for Solid State Science, Physical Sciences, Arizona State University, Tempe, AZ 85287–8301, USA
[i] School of Geographical and Earth Sciences, University of Glasgow, Gregory, Lilybank Gardens, Glasgow, G12 8QQ, UK
[j] University of Utah, Department of Geology and Geophysics, 115 S 1460 E (FASB), Salt Lake City, UT 84112, USA
[k] Department of Palaeobiology, Swedish Museum of Natural History, Stockholm, Sweden
[l] Natural History Museum, Burgring 7, 1010 Vienna, Austria
[m] Department of Lithospheric Research, University of Vienna, Althanstrasse 14, A–1090 Vienna, Austria
[n] Biogéosciences, UMR 6282, CNRS, University of Bourgogne Franche–Comté, 6 boulevard Gabriel, Dijon F–21000, France
[o] Instituto de Geofisica, Universidad Nacional Autónoma de México, Cd. Universitaria, Coyoacán Ciudad de México C. P. 04510, Mexico
[p] Japan Agency for Marine–Earth Science and Technology, 2–15, Natsushima–cho, Yokosuka–city, Kanagawa 237–0061, Japan
[q] Department of Chemistry, Toho University, Funabashi, Chiba 274–8510, Japan
[r] NERC Argon Isotope Facility, Scottish Universities Environmental Research Centre (SUERC), Rankine Avenue, East Kilbride G75 0QF, UK

ARTICLE INFO

Article history:
Received 17 August 2019
Received in revised form 21 November 2019
Accepted 1 December 2019
Available online 13 January 2020

Handling Editor: J.G. Meert

Keywords:
Peri–Gondwanan realm
Chicxulub impact crater
Slab breakoff
Pangea

ABSTRACT

The Late Paleozoic tectono–magmatic history and basement of the Maya block are poorly understood due to the lack of exposures of coeval magmatic rocks in the region. Recently, IODP–ICDP Expedition 364 recovered drill core samples at borehole M0077A from the peak ring of the Chicxulub impact crater, offshore of the Yucatán peninsula in the Gulf of México, have been studied comprehensively. In the lowermost ~600 m of the drill core, impact–deformed granitoids, and minor felsite and dolerite dykes are intercalated with impact melts and breccias. Zircon U-Pb dating of granitoids yielded ages of around 326 ± 5 Ma, representing the first recovery of Late Paleozoic magmatic rocks from the Maya block, which could be genetically related to the convergence of Laurentia and Gondwana. The granitoids show the features of high K_2O/Na_2O, La_N/Yb_N and Sr/Y ratios, but very low Yb and Y contents, indicating an adakitic affinity. They are also characterized by slightly positive $\varepsilon Nd_{(326Ma)}$ of 0.17–0.68, intermediate initial $^{87}Sr/^{86}Sr_{(326Ma)}$ of 0.7036–0.7047 and two–stage Nd model age (T_{DM2}) of 1027–1069 Ma, which may indicate a less evolved crustal source. Thus, the adakitic granitoids were probably generated by partial melting of thickened crust, with source components similar to Neoproterozoic metagabbro in the Carolina block (Pan–African Orogeny materials) along Peri–Gondwana. Felsite dykes are shoshonitic with typical continental arc features that are sourced from a metasomatic mantle wedge by slab–fluids. Dolerite dykes display OIB–type features such as positive Nb and Ta anomalies and low Th_{Npm}/Nb_{Npm}. In our interpretation, the Chicxulub adakitic granitoids of this study are formed by crustal anatexis due to asthenospheric upwelling resulting from slab breakoff. Through comparing sources and processes of Late Paleozoic magmatism along the Peri–Gondwanan realm, a tearing slab breakoff model may explain the discontinuous magmatism that appears to have occurred during the convergence of Laurentia and Gondwana.

* Corresponding author at: State Key Laboratory of Geological Processes and Mineral Resources, Planetary Science Institute, School of Earth Sciences, China University of Geosciences, Wuhan, China.
E-mail addresses: longxiao@cug.edu.cn, lxiao@must.edu.mo (L. Xiao).

https://doi.org/10.1016/j.gr.2019.12.003
1342-937X/

1. Introduction

The Peri–Gondwanan realm located on the eastern edge of the Appalachian–Caledonian orogen (Hibbard et al., 2006; Pollock et al., 2012), comprises the Maya block, Oaxaquia block, Suwannee block and Carolina block, which are crucial components for the assembly of Pangea (Hibbard et al., 2002; Keppie et al., 2012; Mueller et al., 2014; Murphy et al., 2004) (Fig. 1). With the amalgamation of Laurentia and Gondwana, pre–, syn– and post–collisional magmatism are expected to be distributed extensively along the Peri–Gondwanan realm, while the Late Paleozoic magmatism is spatially distributed and occurs as: (1) pyroclastic rocks in sedimentary formations or intrusions within the Oaxaquia block; (2) intrusions discovered by boreholes in the Suwannee block; and (3) widely dispersed granitoids in the Carolina block (Centeno-García, 2016; Heatherington et al., 2010; Lopez and Cameron, 1997; Ortega-Gutiérrez et al., 2018; Poole et al., 2005; Samson et al., 1995a; Speer and Hoff, 1997) (Fig. 1). The Maya block was located within the central region of the Peri–Gondwanan realm during the Late Paleozoic, but few Late Paleozoic outcrops are known so far (Centeno-García, 2016; Marton and Buffler, 1994). Integrated International Ocean Discovery Program–International Continental Scientific Drilling Program (IODP–ICDP) Expedition 364 borehole M0077A, located offshore in the Gulf of México, recovered relatively continuous granitoids and dykes in drill cores from the 200 km diameter K–Pg Chicxulub impact crater (Morgan et al., 2016). These basement rocks were uplifted during the impact event from a pre–impact depth of 8 to 10 km (Riller et al., 2018) and provide crucial information about the record of Late Paleozoic magmatism in the Maya block and its relationship with other Late Paleozoic magmatism along the Peri–Gondwanan realm during the assembly of Pangea.

In the Marathon–Ouachita–Appalachian orogen, the Late Paleozoic magmatic events, especially in the Carolina and Suwannee blocks (Fig. 1), are argued to reflect crustal anataxis related to thickened crust and lithospheric mantle delamination (Heatherington et al., 2010; Sacks and Secor, 1990; Samson et al., 1995a), or coinciding with contemporaneous strike–slip faulting (Speer and Hoff, 1997; Speer et al., 1994), whereas in the Oaxaquia block, they are attributed to coeval continental arc magmatism (Dickinson and Lawton, 2001; Lopez and Cameron, 1997; McKee et al., 1988, 1999). There, may, thus be some petrogenetic and tectonic divergences between areas, depending on differences in original rock composition and/or locations along the Peri–Gondwanan realm during the assembly of Pangea. Alternatively, a transpressional model could explain the lack of continental arc magmatism in the Carolina and Suwannee blocks (Mueller et al., 2014), however, the coeval continental arc magmatism in the Oaxaquia block cannot be well constrained in this model (Fig. 1). Since the Maya block was situated between the Oaxaquia and Suwannee blocks, according to the paleogeographic reconstruction for the Late Paleozoic of Ortega-Gutiérrez et al. (2018), magmatism in the Maya block during that period is critical in determining whether there was a continuous delamination from east to west along the Marathon–Ouachita–Appalachian orogen.

The study of magmatic suites can effectively reveal sources through the analysis of the contributions of crust and mantle. Outcrops of high–

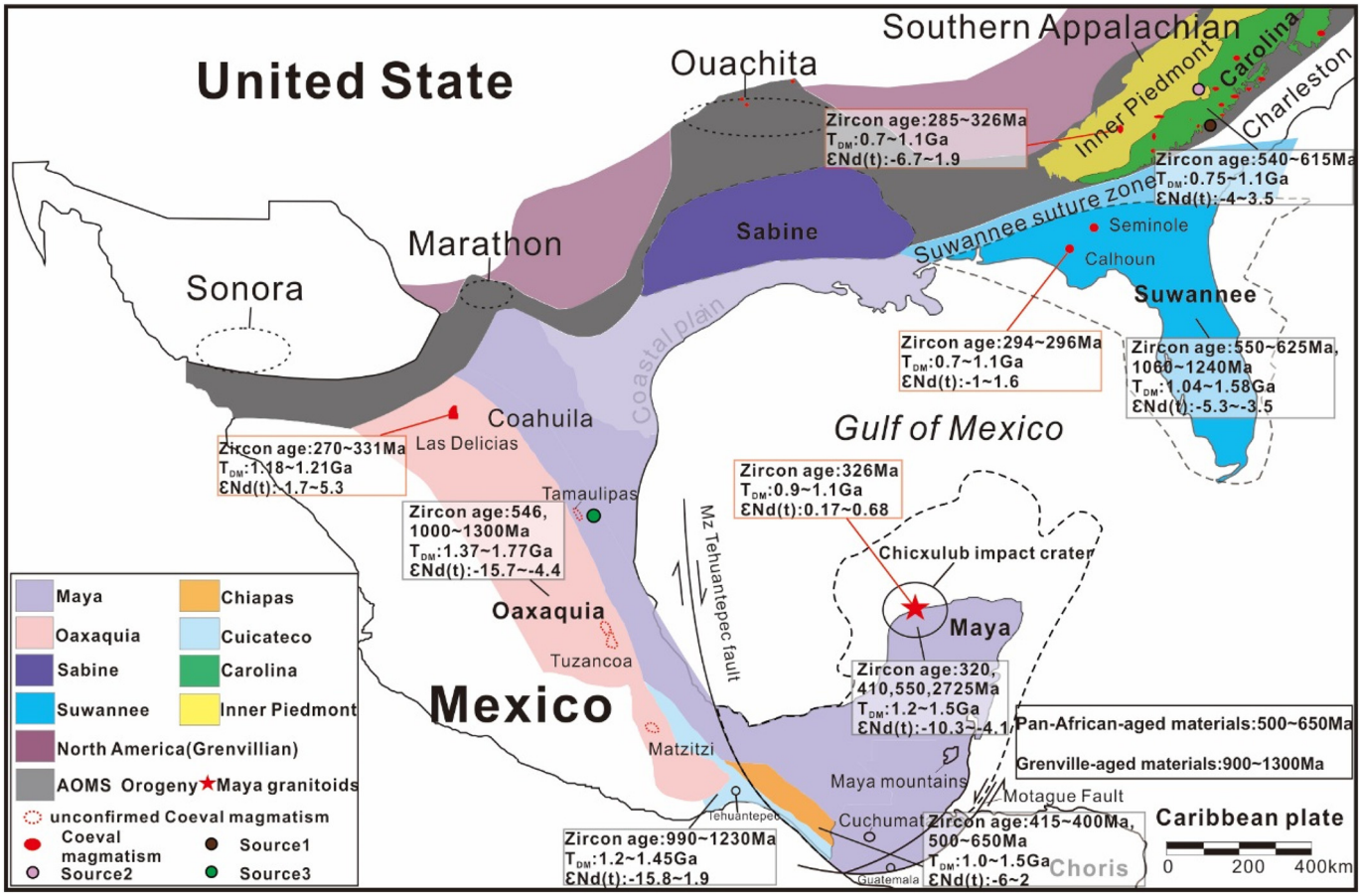

Fig. 1. Sketched geological map of central America modified from Centeno-García (2016); Clift et al. (2017); Ortega-Gutiérrez et al. (2018); Poole et al. (2005) and Dickinson (2009). The southern Appalachian region mainly consists of the Carolina and Inner Piedmont blocks, and the Carolina block refers to the Carolina zone mentioned in Hibbard et al. (2002); Hibbard et al. (2007) and Pollock et al. (2012), the Suwanee suture zone is from Mueller et al. (2014). Late Paleozoic magmatic rocks are according to Heatherington et al. (2010); Lopez and Cameron (1997); McKee et al. (1988, 1999); Samson et al. (1995a); Speer and Hoff (1997); Speer et al. (1994). Zircon ages and Nd isotope data of other areas are from Keppie et al. (2012); Martens et al. (2010); Pollock et al. (2012); Weber et al. (2012). The site of Motague Fault is from Simon-Labric et al. (2013) and the site of Mz Tehuantepec fault is from Dickinson and Lawton (2001). The Grenville-aged materials represent 1.3–0.9 Ga rocks with T_{DM} of 2.02–1.35 Ga, while the Pan-African-aged materials represent 650–500 Ma rocks with T_{DM} of 1.5–0.9 Ga.

grade metamorphic rocks to the south of our study area show that the southern Maya block's basement is dominated by Grenville–aged, Pan–African–aged, and Acadian–aged materials (Keppie et al., 2012; Kring, 2005; Kring et al., 2004; Schmieder et al., 2017b; Steiner and Walker, 1996; Weber and Hecht, 2003; Weber et al., 2008). The northern Maya block is covered by Mesozoic carbonates and evaporates, but the basement samples are found close to the surface as clasts within Chicxulub impact breccias, and are mainly composed of Ediacaran arc materials (Keppie et al., 2011). Moreover, the granitic plutons in the Maya mountains have zircon ages from Late Silurian to Early Devonian (Weber et al., 2012), which could also be the possible basement in the northern Maya block. In the other blocks of the Peri–Gondwana realm, the Oaxaquia block is typical of Grenville–aged basement while Suwannee and Carolina blocks feature the Pan–African–aged basement (Heatherington et al., 1996; Heatherington and Mueller, 2003; Ortega-Gutiérrez et al., 2018; Samson et al., 1995b). Therefore, the differences of basement within the Peri–Gondwanna realm (Oaxaquia, Maya, Suwannee and Carolina blocks) need further investigation (Keppie and Keppie, 2013).

In this study, geochronological and geochemical analyses of Late Paleozoic granitoid cores from IODP-ICDP borehole M0077A in the Maya block are compared with similar studies of coeval magmatism in the Oaxaquia block (331–270 Ma), the Suwannee block (296–294 Ma) and the Carolina block (335–285 Ma) (Fig. 1). Subsequently, an equilibrium melting simulation was used to assess the possible source of Chicxulub granitoids and detailed analyses of the magmatic divergence in the Oaxaquia, Carolina and Suwannee blocks were performed to elucidate the lithological basement features. Finally, an integrated slab breakoff model has been developed to explain the formation mechanisms of magma within each block.

2. Geological setting

The Peri–Gondwanan realm is composed of an array of blocks with Gondwanan affinity and separated from Gondwana during the Early Paleozoic during the formation of the Rheic Ocean and closure of the Iapetus Ocean, which is typically composed of Ediacaran arc (650–500 Ma) magmatic rocks (Keppie et al., 2011; Keppie et al., 2012; Pollock et al., 2011). This study mainly focuses on the Late Paleozoic magmatism in the Marathon–Ouachita–Appalachian orogenic belts, located in the Oaxaquia, Maya, Suwannee and Carolina blocks, respectively. Thus, since the basement serves a considerable function on the attributes of these magmatic rocks, respective basement features of the Oaxaquia, Maya, Suwannee and Carolina blocks are revisited below.

2.1. Maya block

The Maya block is proximal to the Caribbean plate and includes the Yucatán peninsula, the coastal plain of the western and northern Gulf of México, the eastern part of Isthmus Tehuantepec, the Chiapas complex and the northern Guatemala (Weber et al., 2012). The pre–Mesozoic materials of the Maya block are identified by high grade metamorphic rocks in the Chiapas and the Cuicateco (Guichicovi) Complexes (Keppie et al., 2012), and rock fragments excavated by the end–Cretaceous Chicxulub impact. The Chiapas complex mainly includes medium to high–grade metamorphic rocks intruded by less deformed granitoids (Schaaf et al., 2002; Weber et al., 2008), and the detrital zircons reveal ages of 500–650 Ma and 1.0–1.2 Ga in the Carboniferous sedimentary formations (Weber et al., 2008). The single–stage Nd model ages (T_{DM1}) in this area are 1.56–0.94 Ga (Schaaf et al., 2002). In the Cuicateco Complex, parametamorphic rocks and AMCG suite (anorthosite–mangerite–charnockite–granitoids) are dated at 1.2–0.9 Ga (Fig. 2), and their T_{DM1} are 1.63–1.35 Ga (Weber and Köhler, 1999). The fragments excavated by the ~ 66 Ma Chicxulub impact event (Kring, 2005; Kring et al., 2004) consist of Late Paleozoic sedimentary and volcanic rocks (330–290 Ma) in the Yucatán–1 borehole (Marton and Buffler, 1994), and the Yucatán–6 borehole recovered target rocks (550–465 Ma, 418 Ma) (Kamo and Krogh, 1995; Krogh et al., 1993a; Krogh et al., 1993b), of which Ediacaran granitic gneiss clasts reveal a T_{DM1} age of 1.4–0.7 Ga (Kettrup and Deutsch, 2003; Kettrup et al., 2000). In addition, the Yaxcopoil–1 borehole recovered Ediacaran volcanic arc rocks (545 Ma) (Keppie et al., 2011) and Paleozoic clasts (536–395 Ma) (Schmieder et al., 2017b). Therefore, the basement of the Maya block may mainly be composed of Pan–African–aged (650–500 Ma) and Grenville–aged materials (1.3–0.9 Ga).

2.2. Oaxaquia block

Adjacent to the western part of the Maya block lies the Oaxaquia block, which is a Mesoproterozoic block consisting of medium to high grade metamorphic rocks with 1.1 Ga AMCG suite rocks and around 1.0 Ga pegmatites exposed discontinuously along the eastern margin of México (Ortega-Gutiérrez et al., 2018; Ortega-Gutierrez et al., 1995). The zircon ages of lower crust xenoliths and exposed metamorphic rocks in the Oaxaquia block are 1.3–0.92 Ga, and T_{DM1} model ages of these basement rocks range from 2.02 to 1.35 Ga, representing a Grenville–aged endmember called Oaxaquian basement (Keppie et al., 2012; Ortega-Gutiérrez et al., 2018; Ruiz et al., 1988a; Ruiz et al., 1988b; Weber and Köhler, 1999) (Fig. 2). In addition, McKee et al. (1999) reported the Las Delicias arc magmatism (331–270 Ma) in the Oaxaquia block. Their specific chronological and geochemical analysis was conducted by Lopez and Cameron (1997), who demonstrated the features of continental arc magmatism related to the Ouachita–Marathon orogeny coinciding with the detrital zircons in the Marathon foreland basin (Gleason et al., 2007; Shaulis et al., 2012), while some Late Paleozoic magmatism in the Oaxaquia block could be linked to eastward subduction of the Pacific ocean along Pangea (Rosales-Lagarde et al., 2005; Torres et al., 1999) (Fig. 1). Thus, the Oaxaquia block appears to be mainly composed of Grenville–aged basement with some Late Paleozoic continental arc materials.

2.3. Suwannee block

Apart from the overlying Mesozoic and younger rocks of the Gulf and Atlantic coastal plains, a range of Neoproterozoic to Middle Paleozoic rocks comprise the Suwannee block (Heatherington et al., 1996; Heatherington and Mueller, 1999) (Fig. 2). Neoproterozoic volcanic and plutonic rocks (~ 550 Ma) constitute the basement extending beneath the east and southeast of the Suwannee block with the T_{DM1} of 1.58–1.04 Ga (Heatherington et al., 1996; Heatherington et al., 1997; Heatherington et al., 2010; Keppie et al., 2012; Mueller et al., 1994). The minor post–collisional granitoids from two drill holes in southwestern Georgia and northern Florida yielded ages of 294 Ma and 296 Ma, respectively, and they are related to a post–collisional lithospheric collapse (Heatherington et al., 2010; Mueller et al., 2014). Therefore, the Suwannee block contains more juvenile materials compared to the Oaxaquia block based on the lower T_{DM1}.

2.4. Carolina block

The Carolina block and Inner Piedmont constitute parts of the southern Appalachian region (Fig. 1). The Carolina block is predominantly comprised of Neoproterozoic to Early Paleozoic meta–igneous rocks associated with metasedimentary rocks extending from central Virginia southwards to Georgia (Pollock et al., 2010; Samson et al., 1995a), while the Inner Piedmont mainly comprises Mesoproterozoic to Neoproterozoic plutons and high–grade gneisses with a mixed affinity to Gondwana and Laurentia (Fullagar, 2002; Pettingill et al., 1984). Neoproterozoic meta–igneous rocks within the Carolina block represent juvenile crustal materials typified by their higher $\varepsilon Nd_{(t)}$ values (mostly exceeding +3.4) (Samson et al., 1995b) and younger T_{DM1}

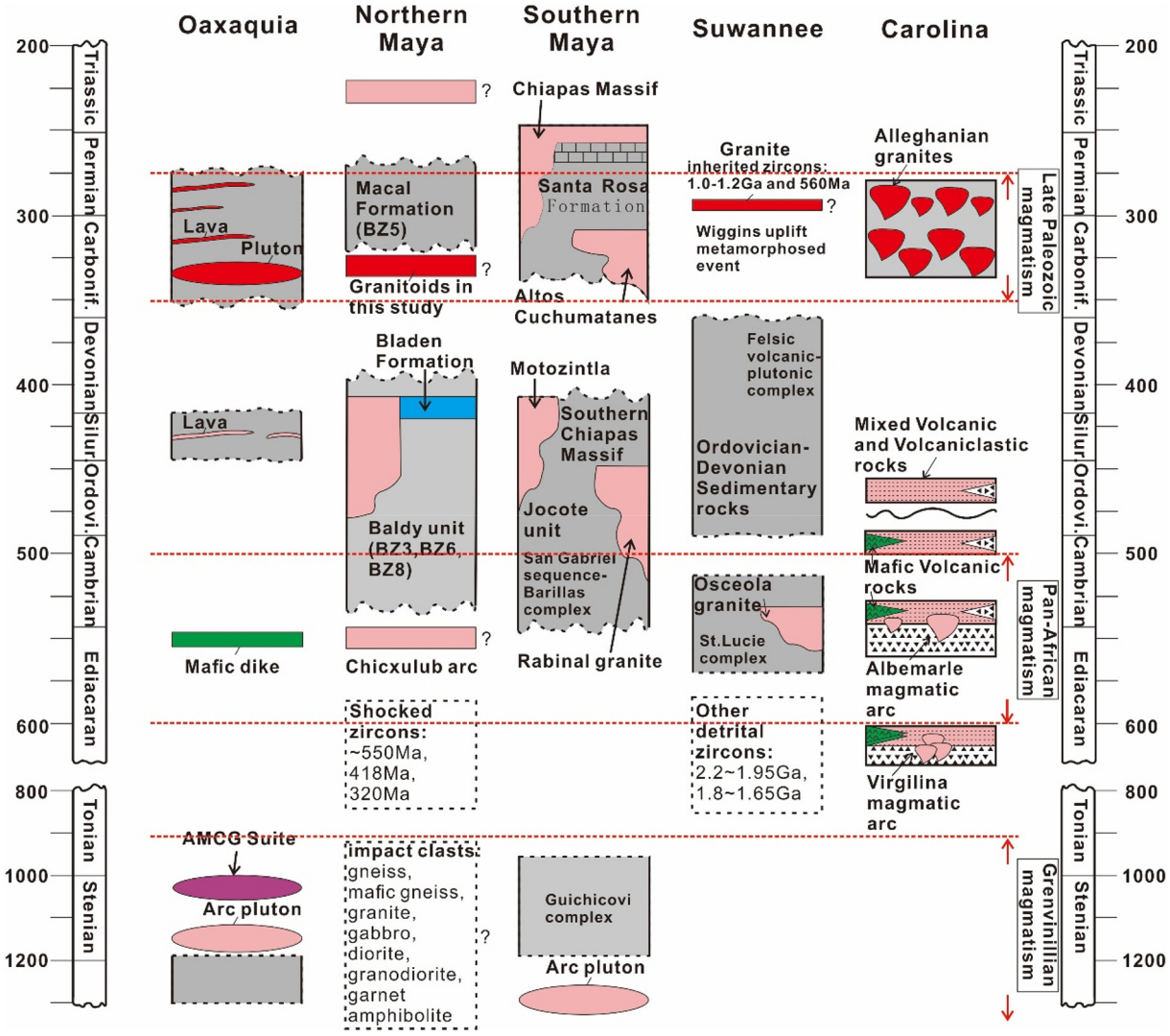

Fig. 2. Sketched stratigraphic columns for the Oaxaquia (Keppie and Ortega-Gutiérrez, 2010; Lopez and Cameron, 1997; Martens et al., 2010), southern and northern Maya (Keppie and Ortega-Gutiérrez, 2010; Kring, 2005; Kring et al., 2004; Martens et al., 2010; Weber et al., 2012), Suwannee (Dallmeyer, 1989; Martens et al., 2010; Mueller et al., 1994) and Carolina blocks (Hibbard et al., 2002; Hibbard et al., 2007; Martens et al., 2010).

(1.1–0.75 Ga) than Grenville–aged materials (Hibbard et al., 2002; Hibbard et al., 2007; Keppie et al., 2012). Thus, the Carolina–like crust is more juvenile than the Grenville–like crust according to their isotopic features (Keppie et al., 2012; Samson et al., 1995a). During the Late Paleozoic assembly of Pangea, the southern Appalachian region hosted extensive magmatic activity (Alleghanian granites: 335–285 Ma), of which 75% are metaluminous biotite or amphibole biotite granites and 25% are peraluminous granites (Samson et al., 1995a; Speer and Hoff, 1997). These rocks were derived from the Carolina block–like crust and the Grenville–like crust mentioned in Samson et al. (1995a). Therefore, the Carolina block also has a more juvenile basement end–member relative to the Oaxaquian basement.

3. Materials and methods

3.1. Materials

Samples for this study are from the IODP-ICDP Expedition 364 drill cores (Site M0077A) from the peak ring of the Chicxulub impact structure (21°27.009′N, 89°56.962′W), located at about 25 km north–west of the Yucatán Peninsula's coast line (Fig. 3). The drilling project was designed to study the formation mechanism of the peak ring of the Chicxulub impact structure and the post impact sedimentary deposits within the crater through multi–disciplinary methods. The drilling reached to a depth of 1334 mbsf (meters below sea floor), recovering basement as well as overlying impact melt rocks, suevites (breccia with impact melt fragments) and post–impact sediments (Morgan et al., 2016). The drill cores were divided into three main stratigraphic units from top to bottom: (1) Cenozoic sediments (505.7–617.33 mbsf); (2) suevites and impact melt rocks (617.33–747.02 mbsf); (3) granitoids (747.02–1334.69 mbsf) intruded by felsic and mafic dykes such as felsite and dolerite (Fig. 3). Felsite dykes occur at 1123.71–1125.44 mbsf, 1130.61–1132.05 mbsf, 1136.7–1139.51 mbsf and 1159.72–1162.26 mbsf. Dolerite dykes are at 846.42–850.64 mbsf, 853.42–855.21 mbsf, 855.56–866.45 mbsf, 887.05–887.95 mbsf, 912.49–913.34 mbsf, 933.98–938.22 mbsf, 1015.87–1016.36 mbsf, 1026.92–1027.14 mbsf and 1082.17–1082.95 mbsf (Schmieder, 2017). The depth of selected samples for geochemical analyses is shown in Fig. 3 and Supplement 2.

3.2. Methods for major and trace elements and zircon U-Pb dating

Granitoid and dyke samples for major element analyses in this study were ground in an agate mortar to pass a 200 mesh sieve to be examined by wet chemical analysis by acid digestion in the State Key Laboratory of Geological Processes and Mineral Resources (GPMR), China

University of Geosciences, Wuhan (CUG). For the determination of silicon content, the sample solutions were produced from the reaction of ash with sodium hydroxide at 650 °C to generate sodium silicate which was then dissolved in HCl to give silicic acid in solution. For other elements, the sample solutions were prepared from acid digestion by hydrofluoric, hydrochloric, sulphuric and nitric acid sequentially. The ten major elements were quantified using the Atomic Absorption Spectroscopy for Mg (<10 wt%), Mn, K, Na and Ca, the spectrophotometry for Si, Fe, Ti, P, and EDTA titration for Al and Mg (>10 wt%). The relative errors were yielded of <0.5% for Si, Mg, Fe, Ti, Mn, K and Na, and <2% for Al, the reference standard is according to GB/T14506-2010 in China.

Trace elements analyzed in the GPMR–CUG were conducted using an Agilent 7500a Inductively coupled plasma mass spectrometer (ICP–MS). The detailed sample–digesting procedures in the GPMR–CUG for trace elements analyses are as follows: (1) Homogenized sample powders were placed in an oven at 105 °C for 12 h to fully dry, (2) 50 mg of sample powder was weighed and digested using 1 ml HNO_3 and 1 ml HF in a Teflon bomb, which was put in a stainless steel pressure jacket and heated to 190 °C for at least 24 h, (3) the Teflon bombs were opened for drying on a hotplate at 140 °C and 1 ml HNO_3 was added and evaporated to dryness again, (4) 1 ml of HNO_3, 1 ml of deionized water and 1 ml internal standard solution of 1 ppm In were added, and the Teflon bomb was placed in an oven at 190 °C for at least 12 h. The final solutions were transferred into a polyethylene bottle and diluted to 100 g by the addition of 2% HNO_3 for analysis. AGV-2, BHVO-2, BCR-2 and RGM-2 were used as reference standards (http://minerals.cr.usgs.gov/geo_chem_stand/, http://georem.mpch-mainz.gwdg.de/ and Govindaraju (1994)), of which AGV-2 yielded relative standard deviation (RSD) of <1% for Nb and Ta, <2% for Sr, Y, Nd, Yb and Lu, <3% for Zr, Ba, La, Ce and Eu, <5% for Rb, Sm and Hf, and the relative deviations (RSD) of other elements are shown in Supplement 2. U-Pb isotope values of zircons were analyzed using an Agilent 7500a ICP–MS coupled with a GeoLas 2005 laser–ablation system and a DUV 193 nm ArF–excimer laser (MicroLAS, Germany) (LA–ICP–MS) in GPMR. Reference zircon 91500 (1063.9 ± 6 Ma) (Wiedenbeck et al., 1995), GJ-1 (600.3 ± 2.6 Ma) (Jackson et al., 2004) and glass NIST 610 were used as external standards for calibration of the mass discrimination and U-Pb isotope fractionation. Each analysis incorporated a background acquisition of approximately 20–30 s followed by 50 s of data acquisition from the sample. In–situ analysis of Hf isotopes and

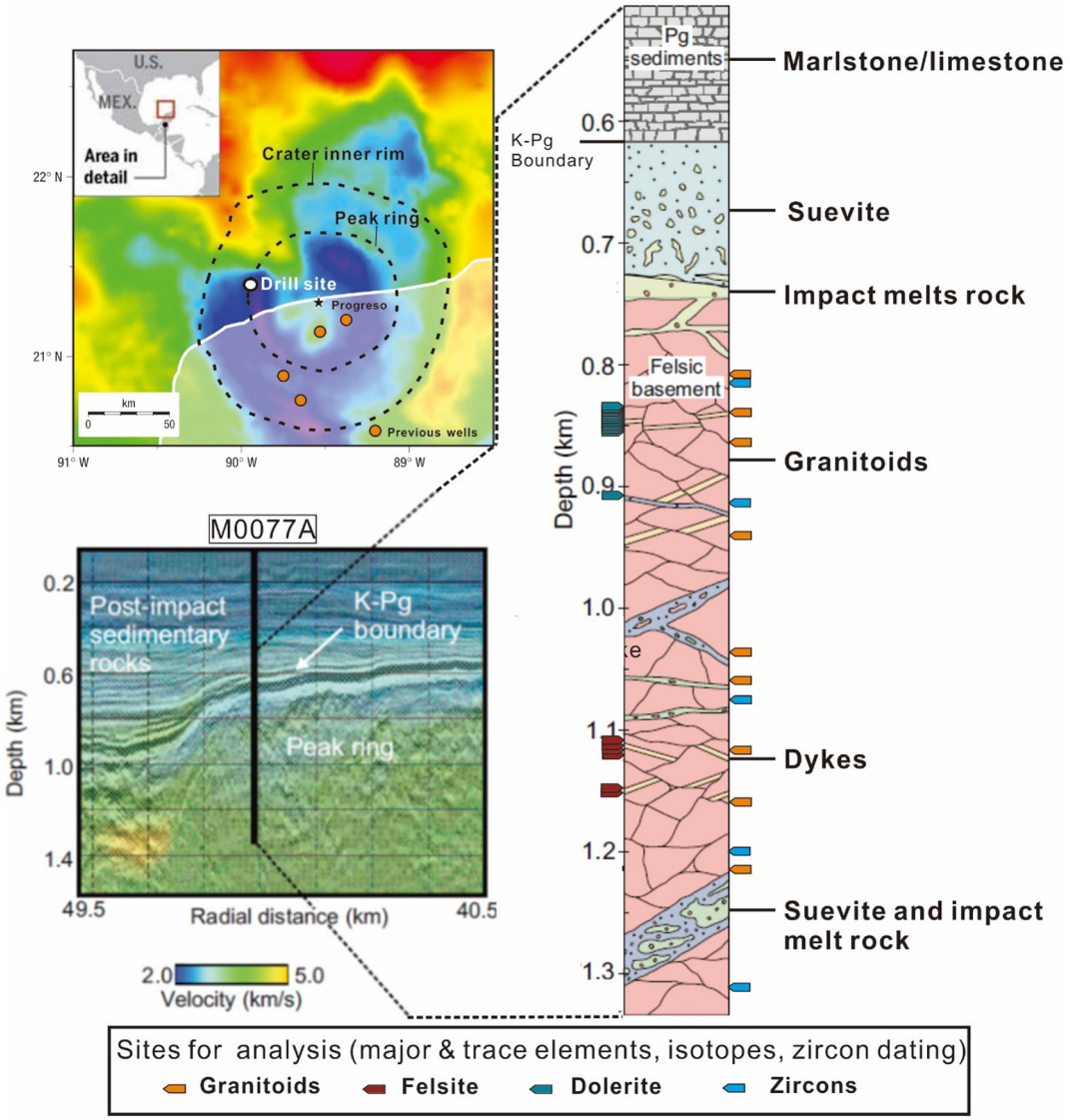

Fig. 3. Map with marked drill site of M0077A and lithostratigraphic context of samples in this borehole. The seismic profile is modified from Morgan et al. (2016) and Gulick et al. (2008), gravity data courtesy of A. Hildebrand and M. Pilkington,

corresponding U-Pb isotope ratios of zircons were conducted using spot sizes of 44 μm and 32 μm, respectively by LA–ICP–MS at the Wuhan Sample Solution Analytical Technology Co., Ltd., Wuhan, China. Operating conditions for the laser ablation system and the ICP–MS instrument and data reduction were done following the methodology described in Zong et al. (2017). The Excel–based software ICPMSDataCal was used to perform off–line selection and integration of background and analyze signals (Liu et al., 2010). Time–drift correction and quantitative calibration for trace element analysis and U-Pb dating followed the protocol outlined by Liu et al. (2010). Concordia diagrams and weighted mean calculations were generated using Isoplot/Ex–ver3 (Ludwig, 2003).

Bremen data including major and trace elements of evenly spaced drill cores were acquired at the MARUM Center for Marine Environmental Sciences, University of Bremen, Germany. These analyses included 194 whole-rock samples, approximately evenly spaced every 3 m, with a minimum weight of 12 g from the depth interval between 748 and 1333 mbsf; 158 of these samples were from granites; 25 samples were from suevite and impact melt rock intercalations; 9 of these samples were from dolerite dykes, one sample was from a felsite dyke, and one from a dacite dyke. Before processing, all samples were dried in an oven at 40 °C for at least 10 h. The samples were then crushed, ground, and homogenized to a fine powder (~20 μm) using an agate mortar and an agate ball mill. Every sample powder was then divided into three subsets and 4 g was used for the measuring of elemental concentrations by energy dispersive X-ray fluorescence (ED-XRF) spectroscopy with a PANalytical Epsilon 3-XL benchtop ED-XRF spectrometer. Replicate analyses of samples and repeated analyses of the certified standard reference materials JB-1b (Terashima et al., 1998) and JG-2 (Imai et al., 1995) yielded relative errors of <6% for Na and Nb; <5% for Ba and Cr; <4% for Cu; <3% for P, Mg, Ni, and Y; ≤2% for Si, Ti, and Sr; ≤2% for Al, K, Fe, Ca, Zr, Rb, Pb, and Zn (Gulick et al., 2017). Replicate analyses of samples analyzed in Bremen yielded the following relative errors: <3% for major and minor element concentrations >1 wt%; <10% for trace element concentrations <1 wt% and > 300 ppm, and up to 30% and larger for trace element concentrations <300 ppm.

3.3. Methods for analysis of Sr, Nd and Pb isotopes

Sr, Nd and Pb isotope analyses were conducted on a Neptune multicollector inductively coupled plasma mass spectrometer (MC–ICP–MS) operated in the Isotopic Laboratory of GPMR–CUG. Sample digestion followed the same procedures as the trace elements digestion. For Sr isotope measurements, after the three sample digestion steps mentioned above, we dissolved the sample in 1.5 ml of 2.5 M HCl and conducted centrifugation, the supernatant solution was then loaded into an ion–exchange column packed with AG50W resin. After complete loading of the sample solution, columns were rinsed with 2.5 M HCl to remove matrix elements. Finally, the Sr fraction was eluted using 2.5 M HCl and gently evaporated to dryness prior to mass–spectrometric measurement. The residue was rinsed with 10 ml of 4.0 M HCl and then the REE fraction was eluted using 10 ml of 4.0 M HCl. The REE solution was used to isolate the Nd fraction, evaporated to incipient dryness, and taken up with 0.18 M HCl. The converted REE solution was loaded into an ion–exchange column packed with Eichrom LN resin. After complete loading of the sample solution, columns were rinsed with 0.18 M HCl to remove undesirable matrix elements. Finally, the Nd fraction was eluted using 0.3 M HCl and gently evaporated to dryness prior to mass–spectrometric measurement. The analytical techniques for Sr-Nd isotopes and analytical precision are the same as those of Liu et al. (2004) and Gao et al. (2004). After the measured $^{86}Sr/^{88}Sr$ and $^{146}Nd/^{144}Nd$ ratios were internally normalized to 0.7219 and 0.51194, respectively, NBS SRM 987 yielded $^{87}Sr/^{86}Sr = 0.710295 \pm 0.000010$ ($n = 10$) (referenced value: 0.710241 ± 0.000017 from Thirlwall (1991)), while JNdi-1 yielded $^{143}Nd/^{144}Nd = 0.512112 \pm 0.000008$ (n = 10) (referenced value: 0.512115 ± 0.000007 from Tanaka et al. (2000)). For the Pb isotope analyses, powder samples also underwent the procedure steps (1 to 3) for trace elements digestion, followed by dissolution in 1 ml of 1 M HBr. After centrifugation, the supernatant solution was loaded into an ion–exchange column packed with AG resin. Columns were rinsed with 1.0 M HBr to remove matrix elements. Finally, the Pb fraction was eluted using 6.0 M HCl and gently evaporated to dryness prior to mass spectrometric measurement. Instrumental mass discrimination correction was carried out via doping with T1 and normalization to a $^{205}Tl/^{203}Tl$ ratio of 2.3872, which is the certified value for NBS SRM 997. NBS SRM 981 was used as the Pb isotopic standard and yielded $^{208}Pb/^{204}Pb = 36.6853 \pm 0.0005$ (referenced value: 36.7262 ± 0.0031), $^{207}Pb/^{204}Pb = 15.4852 \pm 0.0005$ (referenced value: 15.5000 ± 0.0013), and $^{206}Pb/^{204}Pb = 16.9325 \pm 0.0006$ (n = 10) (referenced value: 16.9416 ± 0.0013) (Baker et al., 2004). Total procedural Pb blanks were lower than 50 pg. Rb, Sr, Sm, Nd, Th, U, and Pb contents measured by ICP–MS were used to calculate the initial ratios of $^{87}Rb/^{86}Sr$, $^{147}Sm/^{144}Nd$, $^{208}Pb/^{204}Pb$, $^{207}Pb/^{204}Pb$, and $^{206}Pb/^{204}Pb$.

4. Results

4.1. Petrography

4.1.1. Granitoids

The granitoids in this study exhibit porphyritic texture with 10–20% of the volume represented by coarse phenocrysts of K–feldspar (1–2 cm) and 80–90 vol% by matrix. The matrix comprises medium granular (0.2–0.5 cm) K–feldspar (10–20 vol%), coarse granular (0.5–1 cm) quartz (20–40 vol%), medium granular (0.2–0.5 cm) plagioclase (10–20 vol%) and fine granular (0.02–0.2 cm) biotite (5–10 vol%). Accessory minerals include zircon, titanite, apatite and magnetite, combined <1 vol%. Therefore, these rocks plot mostly in the field of syenogranites, although a few represent monzogranites and quartz syenites (Fig. 4a).

Alteration of granitoids tends to be more pronounced when they are in close proximity to impact melt rocks and fractures. Biotite is often partially or completely altered to chlorite. Meanwhile, plagioclase underwent sericitization. Albitization and feldspathization occurred along fractures close to impact melt intrusions.

4.1.2. Intermediate dykes

The intermediate dykes in this study are mainly represented by felsite dykes with a porphyritic texture. The felsite is composed of 5–10 vol % K–feldspar (0.02–0.05 cm), 10–20 vol% biotite (0.02–0.2 cm) and 5–10 vol% quartz (0.02–0.05 cm) phenocryst and 70–80 vol% matrix; additionally, there are some xenoliths from wall rock such as gneiss and granitoids. Alteration of these dykes is evident with the chloritization of biotite and the occurrence of hydrothermal calcite veins that formed in the late processes, possibly in connection with hydrothermal activities triggered by the Chicxulub impact (Abramov and Kring, 2007; Hecht et al., 2004).

4.1.3. Mafic dykes

The mafic dykes are dolerite with a sub–ophitic to ophitic texture, featuring 30–40 vol% plagioclase (0.2–1 cm) and 10–20 vol% pyroxene (0.2–0.5 cm) phenocryst and matrix (40–60 vol%). Some plagioclase is altered to epidote and most pyroxene is altered to serpentine or chlorite.

4.2. U-Pb zircon geochronology

Zircons of granitoids were selected from five different depths in the drill core: 829.73 mbsf, 927.31 mbsf, 1076.1 mbsf, 1200.26 mbsf and 1328.63 mbsf (Fig. 3). These euhedral to sub–euhedral zircons were mechanically broken with regular to irregular fractures, while oscillatory zoning in zircons is clearly recognized in cathodoluminescence images. We chose highly concordant zircon ages (concordance>95%) to obtain

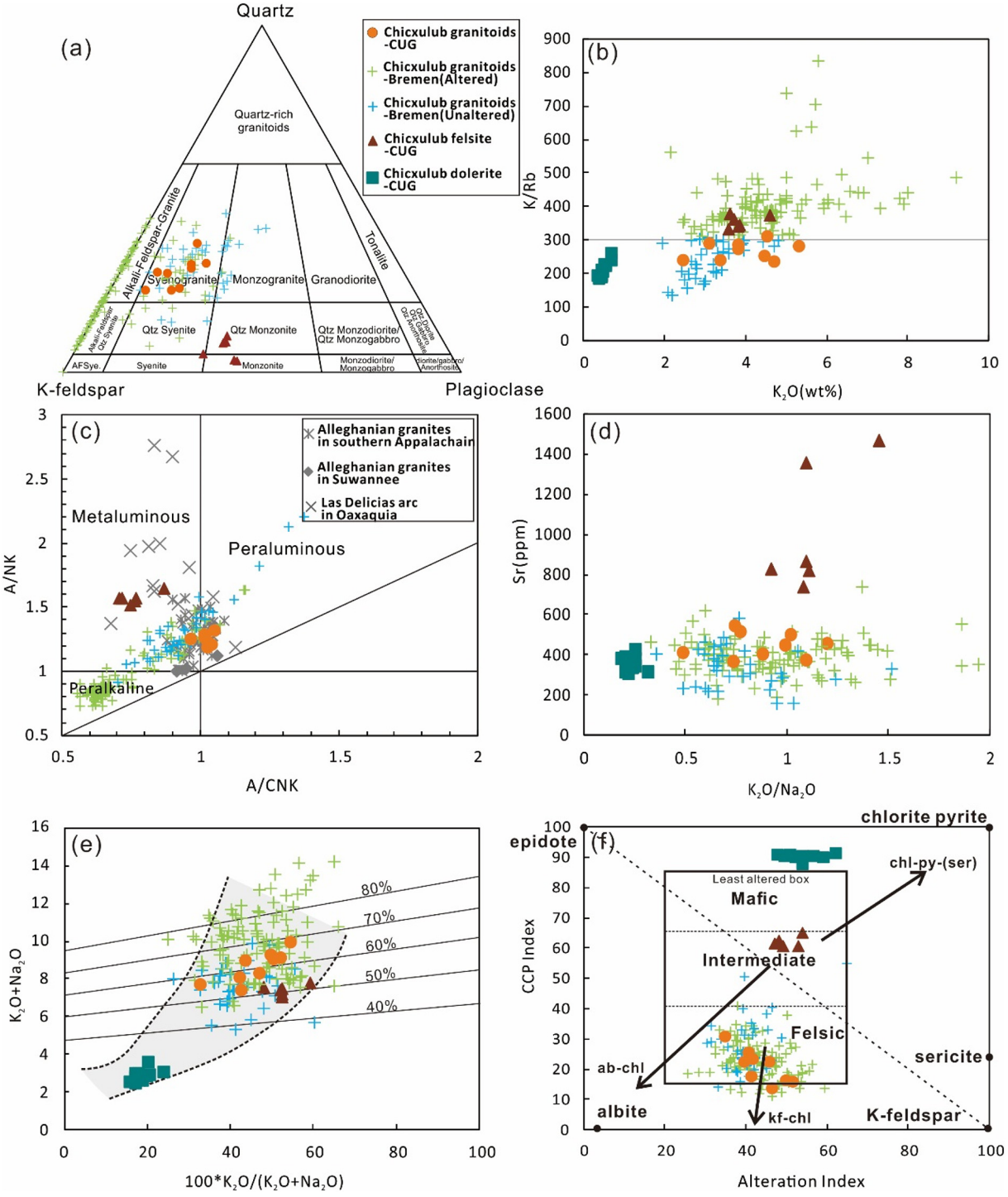

Fig. 4. Covariation diagrams on some major and trace elements. A/CNK = $Al_2O_3/(CaO + K_2O + Na_2O)$, A/NK = $Al_2O_3/(K_2O + Na_2O)$, green and blue crosses represent data acquired at Bremen, which is normalized to 100% (or water–free totals), the grey horizontal line dividing the altered and unaltered data in (b) represents the K/Rb ratios of 300, the straight line in (e) represents the weight percent of alkali feldspar in the rocks (Hughes, 1972). Alteration Index = $100^*(K_2O + MgO)/(K_2O + MgO + Na_2O + CaO)$, CCPI = $100^*(MgO + FeO)/(MgO + FeO + Na_2O + K_2O)$ (Large et al., 2001). (For interpretation of the references to colour in this figure legend, the reader is referred to the web version of this article.)

the weighted mean age (326 ± 5 Ma ($n = 40$)). The results of LA–ICP–MS are reported in Supplement 1 and illustrated in Fig. 5. Inherited zircons are relatively rare but an example with an age of 589 Ma is shown in Fig. 5 a, $^{176}Hf/^{177}Hf$ and $^{176}Lu/^{177}Hf$ ratios of magmatic zircons are 0.282687–0.282747 and 0.00681–0.001382, $\varepsilon Hf_{(326\ Ma)}$ ranges from 3.8 to 6.0, and T_{DM2} are 952–1078 Ma. The inherited zircon has $^{176}Hf/^{177}Hf$ and $^{176}Lu/^{177}Hf$ ratios of 0.282672 and 0.001968 with $\varepsilon Hf_{(326Ma)} = 8.7$ and $T_{DM2} = 984$ Ma (Fig. 5 b).

4.3. Major and trace element geochemistry

4.3.1. Granitoids

The nine granitoid samples that were analyzed show SiO_2 contents of 68.65–73.76 wt%, MgO contents of 0.36–0.98 wt% and K_2O contents of 2.45–5.30 wt%, designating these as part of the medium potassium calc–alkaline series (Fig. 6 e), while most of them are metaluminous (Fig. 6). The K_2O/Na_2O ratios of granitoids range from 0.5 to 1.21.

Major and trace element concentrations are shown in Supplement 2. Hereafter, we refer to these granitoids as Chicxulub granitoids. Trace elements of the Chicxulub granitoids have negative anomalies in Ba, positive anomalies in Sr (362–539 ppm) (Fig. 6 b), and depletions in Nb and Ta compared to N–MORB (Fig. 8 a). The total REE (rare earth elements) content of the Chicxulub granitoids ranges from 44.4 to 81.1 ppm and Eu reveals no obvious positive or negative anomalies (δEu are 0.97–1.04, $\delta Eu = 2^*[Eu]_N/([Sm]_N+[Gd]_N)$, normalized to chondritic values of Sun and McDonough (1989)) (Fig. 8 a). Additionally, the Sr/Y ratios of the Chicxulub granitoids are higher than 40 (55.6–129.8) and La/Yb ratios are over 20 (21.1–44.6). The Y and Yb contents are <18 ppm (3.54–7.24) and 1.9 ppm (0.32–0.70), respectively (Fig. 7 f), making these granitoids highly comparable to adakitic rocks as defined by Chung et al. (2003) and Defant and Drummond (1990).

The Chicxulub granitoids–Bremen data show a large range of major element concentrations especially in the case of Al_2O_3, K_2O, Na_2O, TiO_2 and P_2O_5 (Fig. 6 a, e, f, g, h). The trace element concentrations for elements such as Rb and Ba show similar large variations (Fig. 7 a, c). All these features indicate that the Chicxulub granitoids to some extent underwent hydrothermal alteration presumably before or after the formation of the Chicxulub impact structure (Abramov and Kring, 2007; Schmieder M, 2019). In order to ascertain the alteration of granitoids, we use the K/Rb ratios to divide Bremen data into two sample sets (Fig. 4 b): (1) altered (K/Rb >300) and (2) less altered or unaltered (K/Rb <300) as the K/Rb ratios in unaltered crustal rock is of about 250, and in altered rocks of between 400 and 500 (Helvaci and Griffin, 1983). Thus, alteration processes caused the increase of Na_2O and K_2O content, imparting a peralkaline character to these rocks as shown in Fig. 4 b, c. Theoretically, Sr content is always covariant with CaO for isomorphism (Middelburg et al., 1988). Hence, Sr and CaO concentrations are expected to decrease with the increase of K_2O/Na_2O during feldspathization or other alterations (Saunders and Tuach, 1988). However, the range of Sr content in altered samples did not obviously change compared to unaltered samples (Fig. 4 d). Additionally, according to the $K_2O + Na_2O$ vs $K_2O/(K_2O + Na_2O)$ and the Alteration box (Fig. 4. e, f) (Large et al., 2001), most of the granitoid data plots in the least altered region, indicating that the K_2O/Na_2O ratios still represent the magmatic features of the Chicxulub granitoids. Another explanation for the large range of K/Rb ratios and high content of alkaline elements in Bremen data is that the major and trace elements are affected by the K-feldspar phenocrysts (Fig. 4 a, c).

4.3.2. Intermediate dykes

Six felsite samples have SiO_2 and K_2O contents of 56.37–59.18 wt% and 3.59–4.61 wt% and plot in the shoshonitic series (Fig. 6 e). Mg# ($100^*Mg^{2+}/Mg^{2+}+Fe_t^{2+}$) of felsite are 59–63. Their MgO and CaO contents are 4.96–5.97 wt% and 4.89–6.27 wt% (Fig. 6 b, f), and their Ni contents are 96.9–110 ppm (Fig. 7 d). The shoshonitic felsite has typical features as high K, Ni, Mg#, enriched LILE (large ion lithophile elements) and depleted HFSE (high field strength elements) compared to N–MORB (Fig. 8 b). The total REE of felsite are 387–517 ppm, higher than those in the Chicxulub granitoid host rocks.

4.3.3. Mafic dykes

The dolerite samples plot with medium potassium series (Fig. 6 e) with SiO_2 contents of 45.45–48.26 wt%, and low K_2O and Na_2O contents of 0.40–0.72 wt% and 2.00–2.80 wt%, respectively. They display high MgO and Fe_2O_3 contents of 10.78–13.4 wt% and 11.6–14.72 wt%, respectively, and Mg# are 62–67. In a trace element spider diagram (Fig. 8 a), these dolerites reveal negative anomalies of Th and U, and positive anomalies of Nb, Ta and Sr. Their REE patterns indicate slightly enriched LREE and depleted HREE compared to N–MORB.

4.4. Sr–Nd–Pb isotope characteristics

The Chicxulub granitoid samples have variable present–day $^{87}Sr/^{86}Sr$ (0.706726–0.709886) and $^{143}Nd/^{144}Nd$ (0.512227–0.512253), their initial $^{87}Sr/^{86}Sr_{(326Ma)}$ are 0.7036–0.7047, $\varepsilon Nd_{(326Ma)}$ are 0.17–0.68 and $T_{DM2(326Ma)}$ are 1027–1069 Ma (Depaolo, 1981a; Liew and Hofmann, 1988). These Sr and Nd isotope ratios typically show that nine granitoid samples represent the magmatic features without obvious alteration because these samples have lower initial $^{87}Sr/^{86}Sr$ than the possible wall rock (Grenville–aged rocks) and generally altered samples have higher initial $^{87}Sr/^{86}Sr$ (larger than 0.7080 or even more) (Farmer and DePaolo, 1987). Five felsite samples have Rb/Sr ratios of 0.07–0.13 and Sm/Nd ratios of 0.16–0.17, their $^{87}Sr/^{86}Sr_{(326Ma)}$ and $\varepsilon Nd_{(326Ma)}$ are 0.7045–0.7046 and +1.04–1.22, respectively. Because their $f_{Sm/Nd}$ values are -0.48– -0.50, T_{DM1} (873–915 Ma) are more suitable. Rb/Sr and Sm/Nd ratios in five dolerite samples are 0.05–0.07 and 0.30–0.34, respectively, the initial $^{87}Sr/^{86}Sr_{(326Ma)}$ and $\varepsilon Nd_{(326Ma)}$ are 0.7048–0.7053 and 5.4–7.7, respectively. In addition, the dolerite samples have T_{DM1} and $T_{DM2(326Ma)}$ modelling ages of 908–1771 Ma and 459–644 Ma, respectively, see details in Supplement 3, 4, 5, 6.

Five granitoid samples have $^{206}Pb/^{204}Pb_{(326Ma)}$ = 18.034–18.725, $^{207}Pb/^{204}Pb_{(326Ma)}$ = 15.718–15.774, $^{208}Pb/^{204}Pb_{(326Ma)}$ = 38.162–38.692. Three felsite samples have $^{206}Pb/^{204}Pb_{(326Ma)}$ = 18.416–18.769, $^{207}Pb/^{204}Pb_{(326Ma)}$ = 15.681–15.693, and $^{208}Pb/^{204}Pb_{(326Ma)}$ = 38.414–38.77. The two dolerite samples have $^{206}Pb/^{204}Pb_{(326Ma)}$ = 18.78–18.816, $^{207}Pb/^{204}Pb_{(326Ma)}$ = 15.72–15.865, and

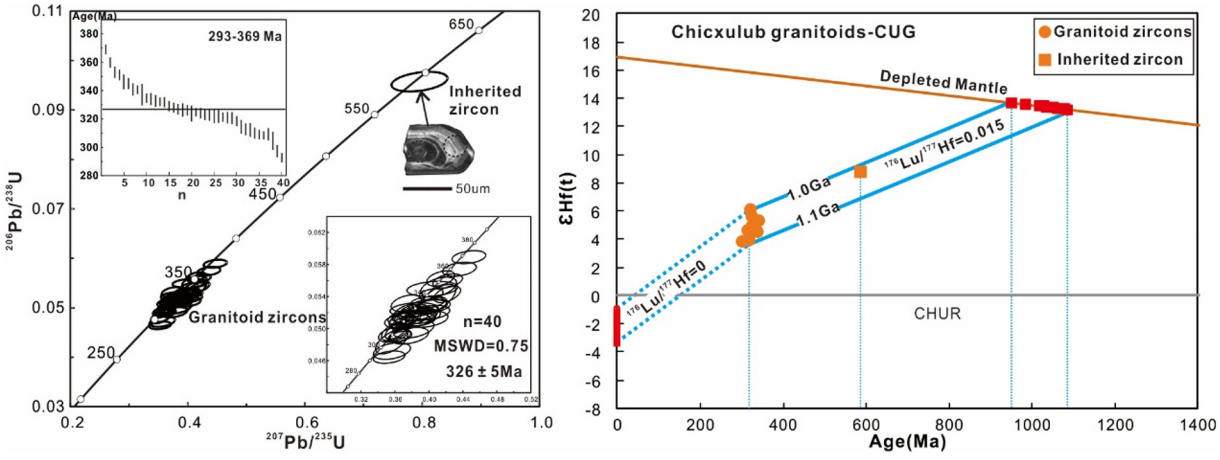

Fig. 5. Ages and εHf (t) of magma and inherited zircons. Crust and mantle Lu-Hf isotopic parameters from Condie (1993). The present–day CHUR values are $^{176}Hf/^{177}Hf_{CHUR} = 0.282772$ and $^{176}Lu/^{177}Hf_{CHUR} = 0.0332$ (Vervoort and Blichert-Toft, 1999) and the calculations for single and two stage model ages are according to Vervoort et al. (2000). The dotted lines ($^{176}Lu/^{177}Hf = 0$) demonstrate that there is no significant radiogenic growth of ^{176}Hf in zircon grains through time.

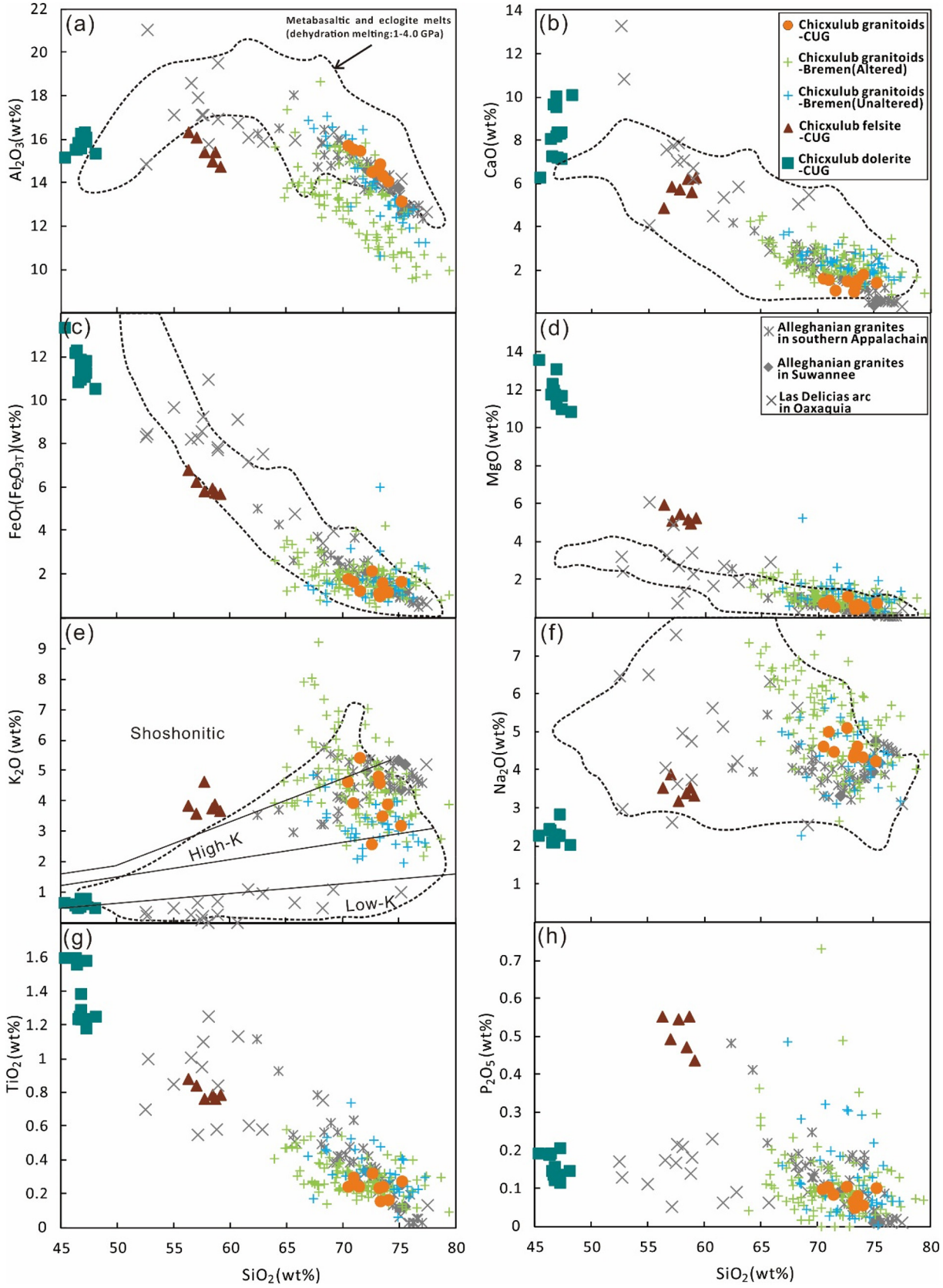

Fig. 6. Bivariate diagrams showing major element variations of the granitoids, felsite and dolerite dykes and coeval magmatism. Data sources: Alleghanian granites from Samson et al. (1995a); Speer and Hoff (1997), Suwannee granites from Heatherington et al. (2010), Oaxaquia magmatic rocks from Lopez and Cameron (1997). Metabasaltic and eclogite melts (dehydration melting: 1–4.0 GPa) region (dotted line) after Wang et al. (2007a).

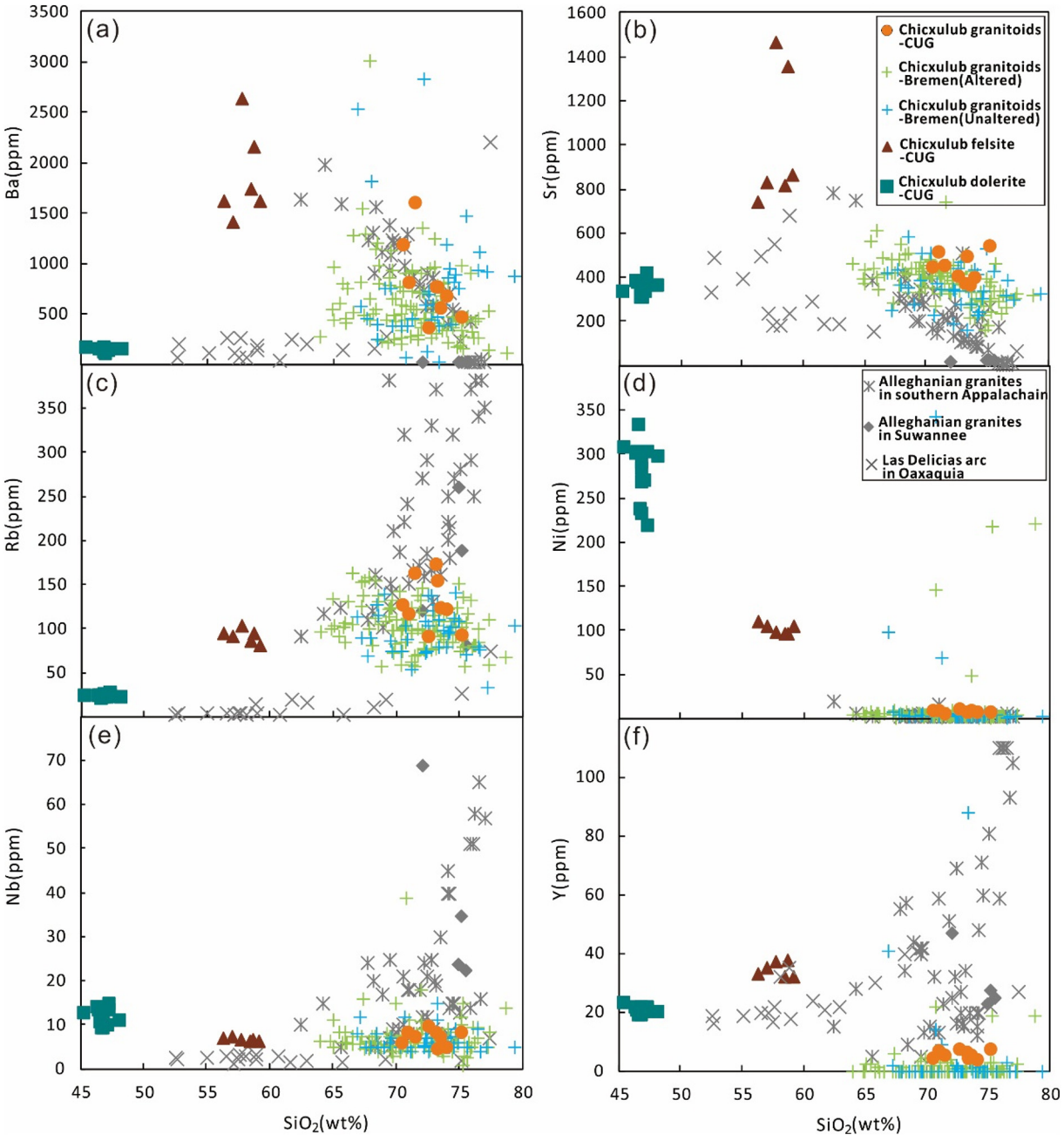

Fig. 7. Bivariate diagrams on trace element variations of granitoids, felsite and dolerite dykes and coeval magmatism, intermediate and mafic dykes. Data sources and symbols are the same as in Fig. 6.

$^{208}Pb/^{204}Pb_{(326Ma)}$ = 38.71–38.904, all these data are shown in Supplement 3, 4, 5, 6.

5. Discussion

5.1. Ages of the Chicxulub granitoids and regional coeval magmatism

In the paleogeographic reconstructions, the Maya block was situated at the convergent margin of Gondwana and Laurentia (Ortega-Gutiérrez et al., 2018), adjacent to the Ouachita Orogen (Poole et al., 2005) (Fig. 1), and is believed to have detached from this orogen during the Mesozoic breakup of Pangea and the opening of the Gulf of México (Marton and Buffler, 1994) (Fig. 1). The Chicxulub granitoids dated at 326 ± 5 Ma reveal a distinct magmatic event in the Marathon–Ouachita Orogen during the Late Paleozoic (Fig. 3). A summary of all the zircon age data used in the present study can be found in Xiao et al. (2017) and Rasmussen et al. (2019). The 341 ± 6 Ma titanite age of Schmieder et al. (2017a,b)), allanite results of Wittmann et al. (2018), and zircon ages from Yax–1 impact breccias in Schmieder et al. (2017b) are also Late Paleozoic. Although there are arc–related materials like meta–andesite and dacite with similar ages in borehole Yucatán–1 (Marton and Buffler, 1994) and tuffs with similar ages (Shaulis et al., 2012), this is the first report of Late Paleozoic ages from a relatively continuous section of the Chicxulub granitoids. In a summary of Mesozoic magmatism in México, Centeno-García (2016) showed that magmatic assemblages are spatially and temporally divergent from this Late

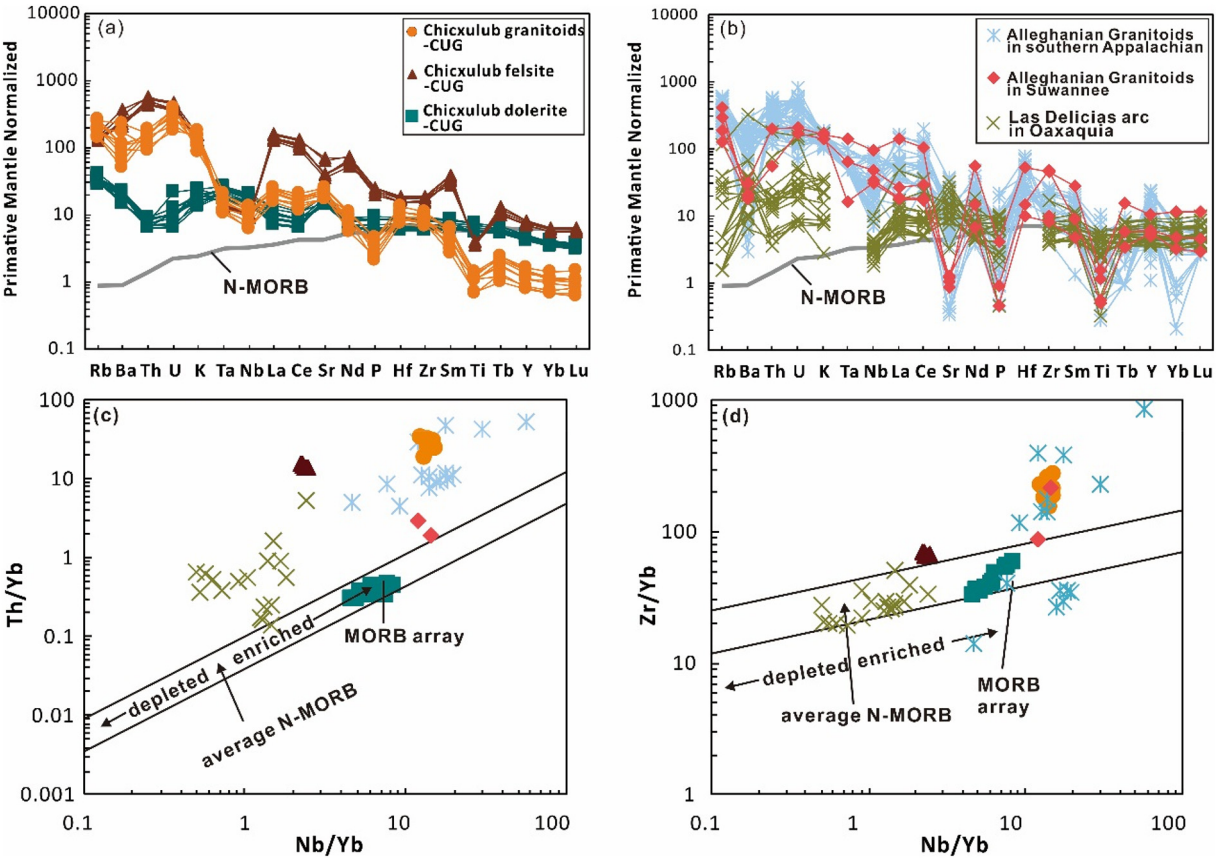

Fig. 8. Primitive–mantle (PM) normalized patterns for Late Paleozoic magmatic rocks for the Carolina, Suwannee and Oaxaquia blocks are from Heatherington et al. (2010); Lopez and Cameron (1997); Speer and Hoff (1997).

Paleozoic magmatism in the Maya block. Thus, these Late Paleozoic magmatic rocks must be related to the Marathon–Ouachita orogeny during the assembly of Pangea.

Magmatic activity has occurred along the Marathon–Ouachita orogen such as the Las Delicias arc within the Oaxaquia block (331–270 Ma); Alleghanian granites in the Suwannee block (296–295 Ma) and in the Carolina block (335–285 Ma) (Fig. 1), illustrating how orogenic products are spatially distributed along the Pangea convergent margin from the Late Mississippian to the Early Permian (Heatherington et al., 2010; Lopez and Cameron, 1997; Samson et al., 1995a). Since the ages of these magmatic events coincide with that of the Chicxulub granitoids, this suggests that they may have a similar petrogenesis. Their magma sources, processes and tectonic models will be further analyzed below.

5.2. Magma sources of the Chicxulub granitoids and dykes

5.2.1. Granitoids

The granitoids in this study are conspicuously similar to typical adakitic rocks shown in Sr/Y versus Y and $(La/Yb)_N$ versus Yb_N diagram (Fig. 9, Moyen (2009)). Equilibrium melting modelling is a simple and ideal way to ascertain the possible source and magma melting conditions. According to the results of equilibrium melting of source A (Archean mafic composite) and source B (MORB) from Defant and Drummond (1990), the granitoids might be sourced from mafic composite which were melted with garnet–bearing amphibolite to eclogite residues. Here, we examine in detail the four possible origins for the granitoids: (1) Typical adakitic rocks formed by melting of a young oceanic slab in a subduction zone (Defant and Drummond, 1990; Martin et al., 2005; Moyen, 2009; Thorkelson and Breitsprecher, 2005); (2) Metasomatic mantle melts that underwent a series of high–pressure AFC (assimilation and fractional crystallization) (Castillo et al., 1999; Manikyamba et al., 2009); (3) Thickened continental crust melted by heating from upwelling asthenospheric mantle during delamination (Chung et al., 2003; Lee et al., 2009; Wang et al., 2007b; Xiao and Clemens, 2007; Xiao et al., 2007); (4) Partial melting of lower crust in an intraplate setting caused by heating from upwelling mantle (Ma et al., 2015; Qian and Hermann, 2013).

The Chicxulub granitoids reveal high K_2O contents and K_2O/Na_2O ratios (Fig. 4 d and Fig. 6 e), which potentially represent a K–rich metabasaltic source (~ 1%) (Rapp and Shimizu, 2002; Xiao and Clemens, 2007). Also, high Rb/Sr ratios (>0.05) indicate an evolved source such as continental crust (Fig. 11 b, d). These features are contrary to melts sourced from oceanic crust slab, which are lower in K content (~ 1.97%), K_2O/Na_2O ratios (~ 0.4) (Martin et al., 2005), and Rb/Sr (<0.05). Moreover, the Chicxulub granitoid $\varepsilon Nd_{(326Ma)}$ are 0.17–0.68, which is lower than the value of MORB that are always larger than 4. According to Zr/Yb vs Nb/Yb (Fig. 8 c, d), the Chicxulub granitoids plot away from the MORB region, indicating that they are unlikely to be the products of the MORB. Therefore, the Chicxulub granitoids are unlikely to be associated with slab melts, so we can discount the first possible explanation for their origin.

Typical high pressure differentiated adakitic rocks are sourced from metasomatic mantle; they feature intermediate or mafic arc rocks, which support differentiation processes (Castillo et al., 1999). The intermediate or mafic arc rocks are quite distinct from the dykes in this study for their different evolution trends (Fig. 6 and Fig. 8 c, d). Also, high pressure differentiated adakitic rocks have similar low K_2O/Na_2O ratios and large SiO_2 content range (Castillo et al., 1999; Macpherson et al., 2006). Consequently, the Chicxulub granitoids are not formed from high pressure differentiation, and we can rule out the second suggestion for their origin.

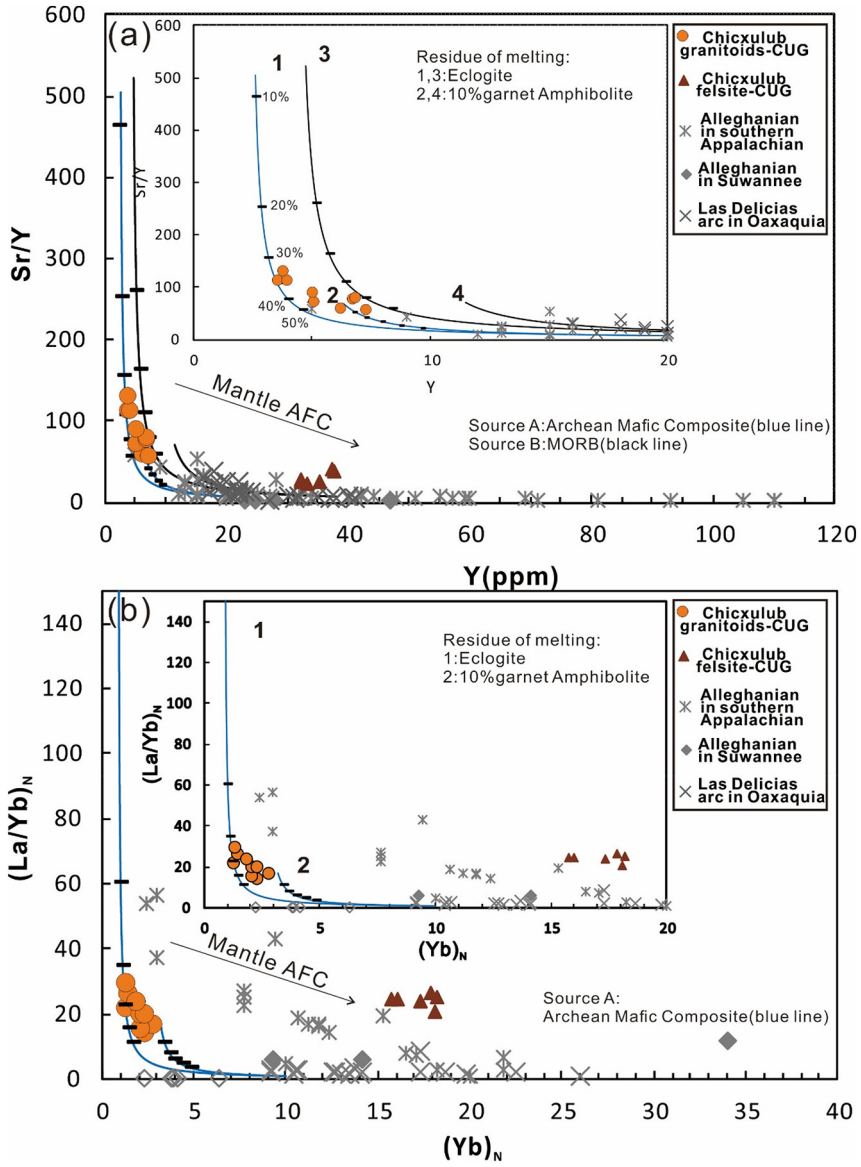

Fig. 9. Sr/Y versus Y and $(La/Yb)_N$ versus Yb_N diagram, curves (1, 2, 3, 4) are from Defant and Drummond (1990), MORB refers to Mid–ocean ridge basalt, AFC refers to assimilation and crystallization processes. La/Yb and Yb are normalized by CI chondrite from Sun and McDonough (1989).

Adakitic melts from intra–continent settings are always indiscernible because they contain the same geochemical features as melts from thickened crust and require ancient crustal sources with the diagnostic features of lower $(Sm/Yb)_{SN}$ and higher Yb_{SN} than typical adakitic rocks from oceanic slabs (Ma et al., 2015; Qian and Hermann, 2013). These features are not evident in granitoids in this study. More importantly, the regional tectonic setting represents a convergent margin of Pangea, which is not consistent with an intra–continent setting.

As for adakitic melts from thickened crust, they have typical features like high K_2O content and high K_2O/Na_2O ratios (Chung et al., 2003; Lee et al., 2009; Wang et al., 2006; Wang et al., 2007a). In addition, relatively higher Rb/Sr, $^{87}Sr/^{86}Sr_{(initial)}$ and lower $\varepsilon Nd_{(t)}$ are also distinct from adakitic rocks sourced from oceanic slabs (Wang et al., 2007a). These kinds of K–rich adakitic rocks tend to have a larger range of Al_2O_3 contents (Lee et al., 2009; Wang et al., 2007a), which agrees with the composition of the Chicxulub granitoids in this study, suggesting adakitic granitoids. However, there are two mechanisms that can lead to the melting of thickened crust: (1) thickened crust or mantle delamination, and (2) slab break off. These two scenarios are discussed in Section 5.4.

5.2.2. Felsite dykes

The felsite dykes exhibit remarkable enrichments in LILE and LREE coupled with depletions in HFSE such as Nb, Ta, and Ti (Fig. 8 a), which are typical features of continental arc rocks (McCulloch and Gamble, 1991). And they are consistent with the continental arc features of both non–conservative elements (e.g. Th/Yb) and conservative elements (e.g. Zr/Yb) mentioned in Pearce and Peate (1995) (Fig. 8 c, d). Additionally, their high K_2O contents, enrichments in LREE and other incompatible elements demonstrate that the source of the felsite dykes are metasomatic mantle by slab fluids, containing K–rich minerals such as amphibole or phlogopite (Petford and Gallagher, 2001; Rapp et al., 1999). Slightly positive $\varepsilon Nd_{(326Ma)} = 1.04–1.20$ indicate a less evolved metasomatic mantle source. In addition, felsite dykes may be contaminated with crustal materials as evidenced by wall rock xenoliths from wall rock within dykes and Pb isotopic features in Fig. 12. Also, based on their REE patterns, the felsite dykes are similar to the shoshonitic rocks related to slab breakoff reported in the Tibet plateau (Lee et al., 2009) and the Alps (Davies and Blanckenburg, 1995), suggesting they may be shoshonitic dykes.

5.2.3. Dolerite dykes

According to the Th/Yb vs Nb/Yb and Zr/Yb vs Nb/Yb diagrams (Fig. 8 c, d), the dolerite samples plot in the E–MORB region, representing an enriched mantle source. The Ce/Y versus Zr/Nb diagram (Supplement 7), suggests that dolerite dykes in this study were possibly derived from spinel peridotite (Hardarson and Fitton, 1991; Xia et al., 2004), which could be the asthenospheric mantle. This is consistent with petrology results of Schmieder et al. (2017), and suggests that the dolerite dykes are a product of magma that was concomitant with the granitoids and felsites, or a different later phase of magmatism than that of the granitoids and felsites.

5.2.4. Constituents of the Northern Maya basement and possible sources for the Chicxulub granitoids

Unlike the southern Maya block, there are no outcrops of high–grade metamorphic rocks in the northern Maya block. The basement of the northern Maya block is mainly composed of Pan–African–aged materials such as mafic tholeiitic dolerite (546 Ma) in the Gd. Victoria area, Grenville–aged low–grade metasedimentary rocks and granodiorite clasts from the Chicxulub impact crater, and Acadian granodiorite in the Altos Cuchumatanes region (480–400 Ma). All these features were presented in Ortega-Gutiérrez et al. (2018).

Zircons within impact breccias at the Chicxulub impact site and the K-Pg boundary ejecta layer may originate from depths of up to 12 km below the pre-impact surface (Kring and Durda, 2002). Three groups of zircon ages reported in previous studies are categorized according to abundance distribution: (1) 545 Ma, (2) 418 Ma, (3) 320 Ma (Kamo and Krogh, 1995; Kamo et al., 2011; Krogh et al., 1993a; Krogh et al., 1993b; Rasmussen et al., 2019; Schmieder et al., 2017b). The 545 Ma zircon ages represent Ediacaran arc materials formed in the Pan–African orogeny, which constitutes the major part of the basement of the Yucatán peninsula/northern Maya block (Keppie et al., 2011), while Keppie and Keppie (2013) support the concept that most of the Yucatán Peninsula/ northern Maya block has a Laurentian affinity. Zircon ages from granitoids in this study (326 Ma) coincide with the aforementioned juvenile ages of zircons in impact breccias. Meanwhile, ages of andesite or dacite in borehole Yucatán–1 are 330–290 Ma (Kring et al., 2004; Marton and Buffler, 1994). The inherited zircon ages of 1210 Ma from the Maya mountain (Steiner and Walker, 1996) and 1100 Ma from the Chicxulub granitoids (Ross et al., 2019) imply that the northern Maya block may also have Grenville–aged materials.

As for Nd and Hf model ages (Fig. 5 b and Fig. 12 b), those for the granitoids in this study range from 1.1 to 0.9 Ga and the majority of the impact breccias in the Chicxulub impact structure show T_{DM1} of 1.45–0.7 Ga, while the T_{DM1} of impact melt rocks are 1.2–1.1 Ga (Keppie et al., 2011; Keppie et al., 2012; Kettrup and Deutsch, 2003; Kettrup et al., 2000). These features also imply that both Pan–African–aged basement and more juvenile materials such as Late Paleozoic orogeny materials were components of the target rock at the Chicxulub impact site. Thus, the major basement component of the northern Maya block appears to be Pan–African–aged materials.

Considering the possible source of the Chicxulub granitoids, several types of Grenville–aged sources such as the high–grade metamorphic rocks outcropping in the southern Maya region and the low–grade metasedimentary clasts in the Chicxulub impactites are not alternatives as their trace elements and Sr-Nd isotope characteristics are contradictory to those of the Chicxulub granitoids in this study (Keppie et al., 2012). Instead, the Pan–African–aged materials are the most probable sources for the Chicxulub granitoids, considering their distribution, chronological, and isotopic features. However, no continuous Pan–African–aged materials have been recovered from the Chicxulub impact structure so far, preventing the comparison of geochemical data. Thus, we chose three Pan–African–aged sources from the northern Maya block and the Carolina block to ascertain the possible starting materials and their residues from equilibrium melting, see Supplement 4 and 5.

The mafic dolerite dykes from the northern Maya block formed by plume–related magmatism during the Pan–African orogeny, the proximal Carolina block also contains Pan–African–aged metabasaltic rocks (Keppie et al., 2011; Samson et al., 1995b), and the ages of Pan–African–aged materials are similar to inherited zircons (589 Ma) in the Chicxulub granitoids (Fig. 5 a, b). Thus, we chose three kinds of Pan–African–aged materials from the northern Maya, northern and southern Carolina block mentioned in Table 1 to ascertain possible or analogous sources for the Chicxulub granitoids. They are both metabasaltic rocks with less evolved Nd isotope values ($\varepsilon Nd_{(t)}$ = +2.6–3.4, +2.0–3.5) (Dennis et al., 2004; Pollock and Hibbard, 2010), theoretically coinciding with the source of the Chicxulub granitoids. Source 1 (metavolcanic arc) and source 3 (dolerite dykes) are enriched in LILE (Rb, Ba), HFSE (Nb, Ta) and HREE (Gd, Y, Lu), but modelling results only partially match the features of the Chicxulub granitoids (Fig. 10 a, b, e, f). Source 2 (Stony Mountain gabbro) is less rich in Rb, Ba, Nb and Ta and obviously more abundant in U and Sr (Fig. 10 c, d), as are the Chicxulub granitoids. Fig. 10 shows the results of varying the degree of partial melting of the starting materials between 1 and 60%. Source 2 (Stony Mountain gabbro, Fig. 10 c, d) produces the best match to the source of the Chicxulub granitoids.

5.3. Magma processes of the Chicxulub granitoids

The Chicxulub granitoids in this study are simulated by melting sources 1 to 3 with six types of residues: the partitioning coefficients and 1–60% partial melting modelling data are shown in Supplement 4, 5 and Fig. 10. Source 2 has a wide range of SiO_2 (36.74–53.23 wt%), Al_2O_3 (9.63–16.1 wt%), MgO (2.13–23.65 wt%), K_2O (0.04–1.46 wt%), Mg# (36–89), Sr contents (79.5–383 ppm) and Y contents (7.33–64.6 ppm), and the results of the melting are compatible with a source melted with garnet in the residue, specifically. The residues are amphibolite (residue 1 and 3) or garnet–bearing granulite (residue 5 and 6) (Fig. 10 b, d, e, f). Moreover, the Nb/Ta ratio is low in the Chicxulub granitoids (Fig. 11 a), which means that rutile does not dominate in melting residues because it would have led to higher Nb/Ta ratios. Positive Sr anomalies and the absence of positive or negative Eu anomalies in the Chicxulub granitoids reveal that plagioclase is either not dominant in residues or plagioclase fractional crystallization is negligible or, possibly, that the high Sr positive anomalies were inherited from the features of the starting sources. All three explanations are consistent with the modelling results (Fig. 10 c, d). Additionally, some low Nb/Ta ratios in the Chicxulub granitoids suggest that either the magma was contaminated by upper crustal materials or that the Nb/Ta ratio in the source rock was lower than the modelled ratio (for the simulations, we use the average Nb/Ta of the source) (Fig. 8 a and Fig. 11 a).

According to the Rb/Ba versus Rb/Sr diagram (Sylvester, 1998) (Fig. 10 d), the magma source of the Chicxulub granitoids was most likely clay–poor material. Likewise, the Pb isotope features indicate that the Chicxulub granitoids are contaminated by more evolved regional materials or late alteration (Fig. 12 c, d), but such contamination does not affect the Sr-Nd isotopic features (Fig. 12 a, b). Additionally, the Chicxulub granitoids have relatively low MgO (<3%), Ni, Y and Nb content as a whole (Fig. 7 d, e, f), thus, the involvement of mantle materials in the generation of the Chicxulub granitoids is not significant. Therefore, these features collectively indicate that the Chicxulub granitoids are sourced from a less evolved lower crustal source (Fig. 12 a, b).

5.4. Geodynamic models for the K–rich adakitic Chicxulub granitoids

K–rich adakitic rocks sourced from thickened continental crust are mainly caused by two mechanisms: delamination of thickened crust or mantle (Chung et al., 2003; Nelson, 1992; Sacks and Secor, 1990; Wang et al., 2006; Wang et al., 2007a) and slab breakoff (Davies and Blanckenburg, 1995; Lee et al., 2009; Sacks and Secor, 1990). In both of these models, asthenospheric upwelling is the cause of heating and

Table 1
Possible sources chosen as starting materials for equilibrium melting, their detailed information from Dennis et al. (2004); Keppie et al. (2006); Pollock and Hibbard (2010). Their sites are marked in Fig. 1.

	Source	Location	Age	$\varepsilon Nd_{(t)}$	Inferred tectonic setting
1	Mafic metavolcanic arc rocks	southern Carolina	540–626 Ma	2.0–3.5	Volcanic arc
2	Stony Mountain gabbro	northern Carolina	530–540 Ma	2.6–3.4	Arc rift–back arc
3	Mafic dolerite dykes	northern Maya	546 Ma	---	Rift, plume–related

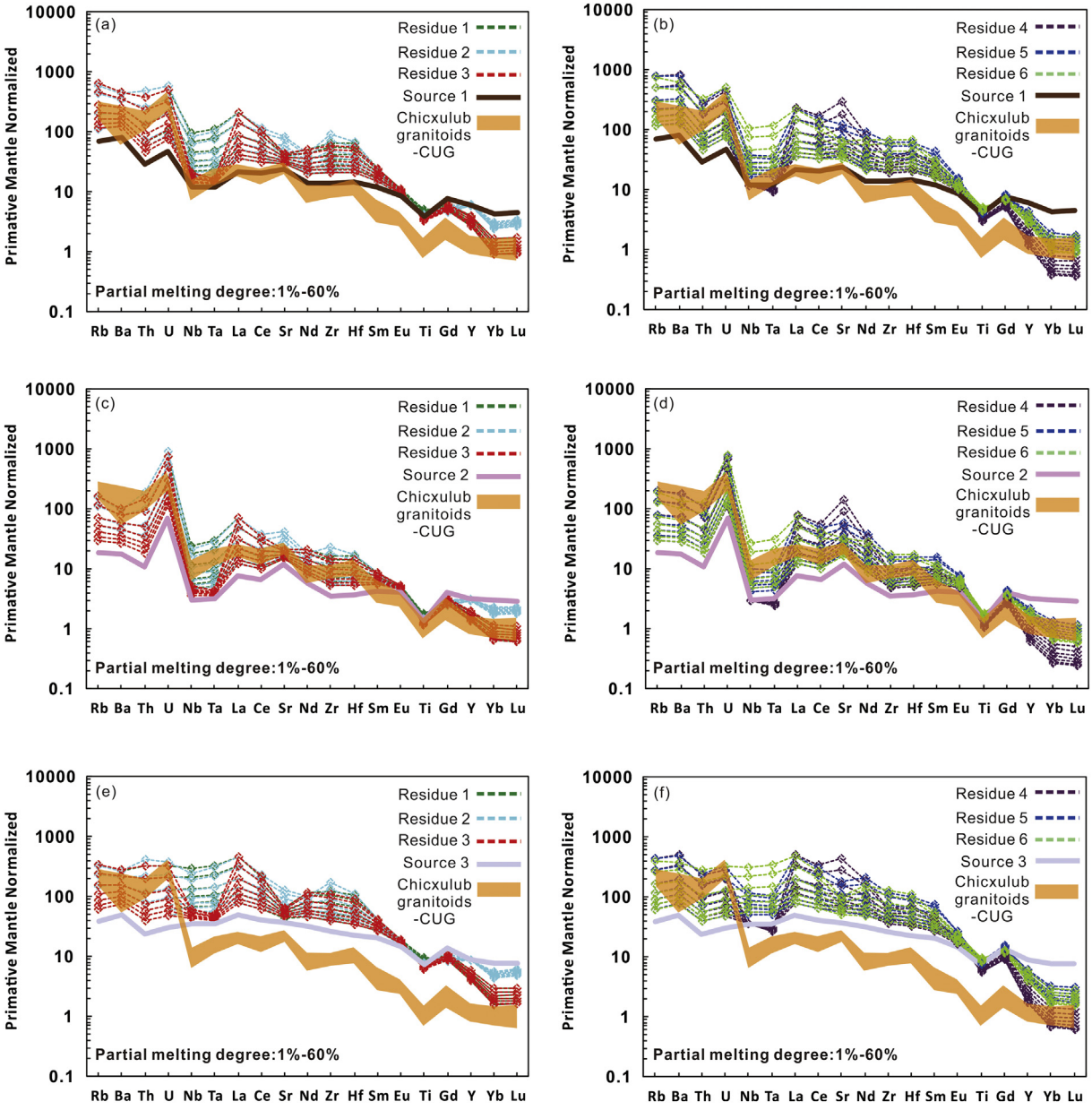

Fig. 10. Primitive–mantle (PM from Sun and McDonough (1989)) normalized patterns for equilibrium melting modelling results: melting sources are average compositions of metamorphic Neoproterozoic volcanic arc basement in southern Carolina (Dennis et al., 2004) (Source 1) (a, b), Stony Mountain metagrabbro in northern Carolina (Pollock and Hibbard, 2010) (Source 2) (c, d) and Mafic dolerite dykes in northern Maya block (Keppie et al., 2006) (Source 3) (e, f). The equilibrium melting models are under the circumstance of six types of residues: 1) 10% garnet Amphibolite (Rutile free): 0.1Grt + 0.75 Amp + 0.15Pl; 2) Amphibolite: 100% Amp; 3) 10% garnet Amphibolite (0.5% Rutile): 0.1Grt + 0.75Cpx + 0.145Pl + 0.005Rt; 4) Eclogite (1% Rutile): 0.3Grt + 0.69Cpx + 0.01Rt, 5) Pyroxenite (2% Ilmenite): 0.08Grt + 0.6Cpx + 0.25Opx + 0.05Pl + 0.02Ilm, 6) Garnet–bearing Granulite: 0.1Grt + 0.3 Amp + 0.3Cpx + 0.2Opx + 0.1Pl. Partition coefficients data: D for garnet, amphibole and clinopyroxene from Severs et al. (2009); Xiong (2006), D for rutile from Xiong et al. (2005), D for plagioclase from Severs et al. (2009), more detailed modelling results are in Supplement 5.

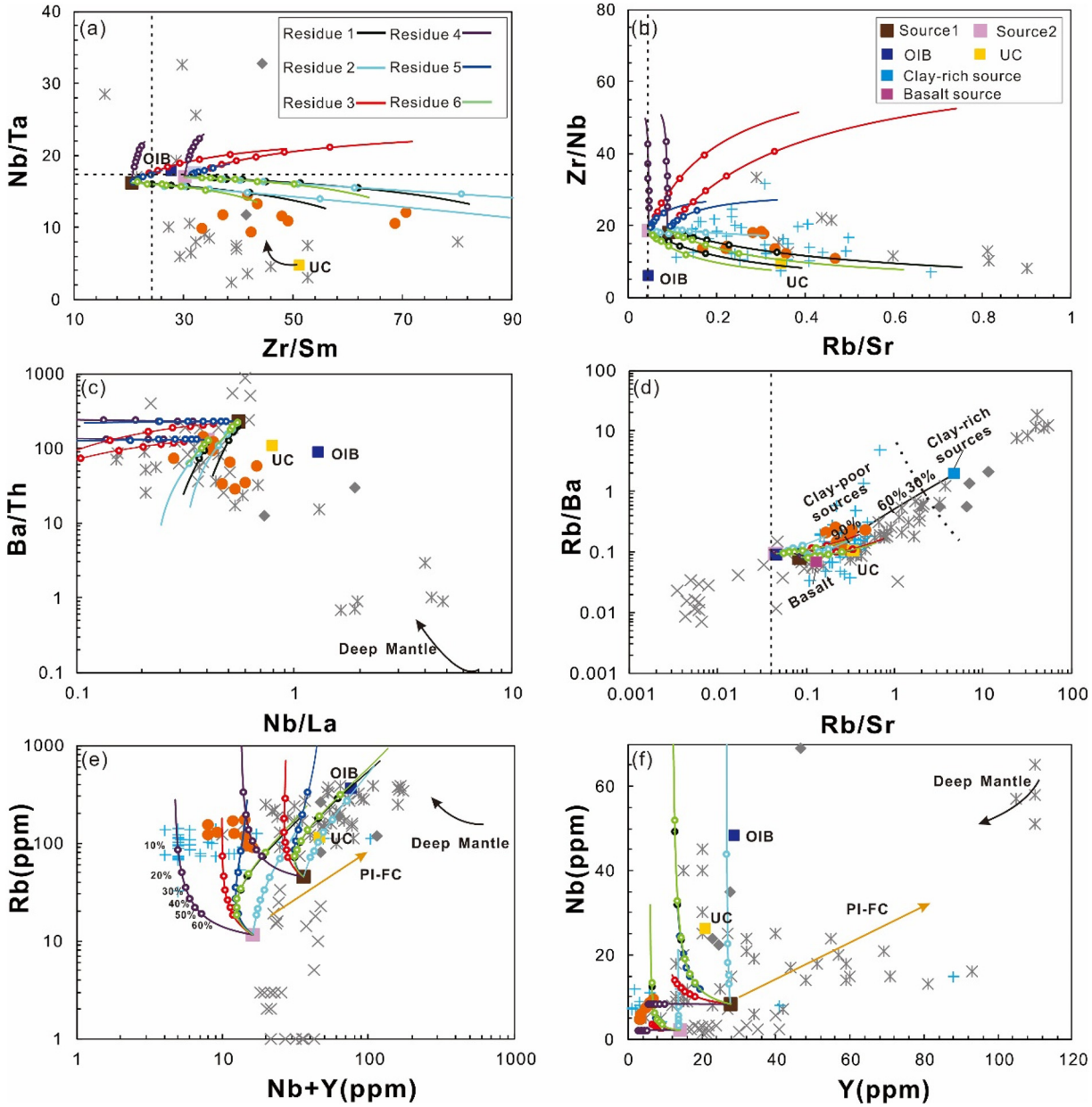

Fig. 11. Equilibrium melting of possible sources from Carolina block. The data source and symbols are the same as Fig. 9, Upper crustal (UC) composition is from Shaw et al. (1976), Ocean island basalt composition (OIB) is from Sun and McDonough (1989). The hollow circles on each equilibrium melting curve represent the degree of partial melting and vary from 10% to 60%. Data sources and symbols are the same as Fig. 6. The vertical dotted lines separate the adakitic rocks (right) and continental arc rocks (left). The horizontal dotted line separates the melting results for eclogite (up) and amphibolite (down) after Martin et al. (2005).

melting of the thickened crust and/or mantle. However, the distribution, type, volume and timing of magma generation are quite different in these two models.

5.4.1. Delamination of thickened crust or mantle

This scenario occurs after collision or during the post collision period due to the collapse of a thickened orogenic root by its high weight (Nelson, 1992). The thickened crust or lithospheric mantle is removed by the difference in density or by mantle convection (Kay and Kay, 1993). K–rich adakitic rocks sourced from thickened lower crust and potassic magmatism derived from lithospheric mantle are typical features of magmatism due to the upwelling asthenosphere (Chung et al., 2003). The key problem with this scenario is that the onset time of thickened crust or mantle delamination is not supported by regional metamorphism and sedimentary records because the formation of the Chicxulub granitoids preceded the main compressional setting (Poole et al., 2005). Although geochemical features of K–rich adakitic rocks in thickened orogenic crust such as the Tibetan Plateau and the Dabie orogenies show a good resemblance to the Chicxulub granitoids, it is unlikely that the Chicxulub granitoids could be formed by the delamination of thickened crust or mantle without there being a period of significant crust and mantle thickening (that generated a crustal thickness of >60 km).

5.4.2. Slab breakoff

Slab breakoff can occur after the collision of two continents, when continental lithosphere starts subducting with the oceanic slab during the initial stage of collision, which may account for much of syn–orogenic magmatism and metamorphism that is observed in orogenic belts (Davies and Blanckenburg, 1995; Sacks and Secor, 1990). The sources of magmatic rocks in this model mainly include the lower crust, metasomatic lithospheric mantle and even the asthenospheric

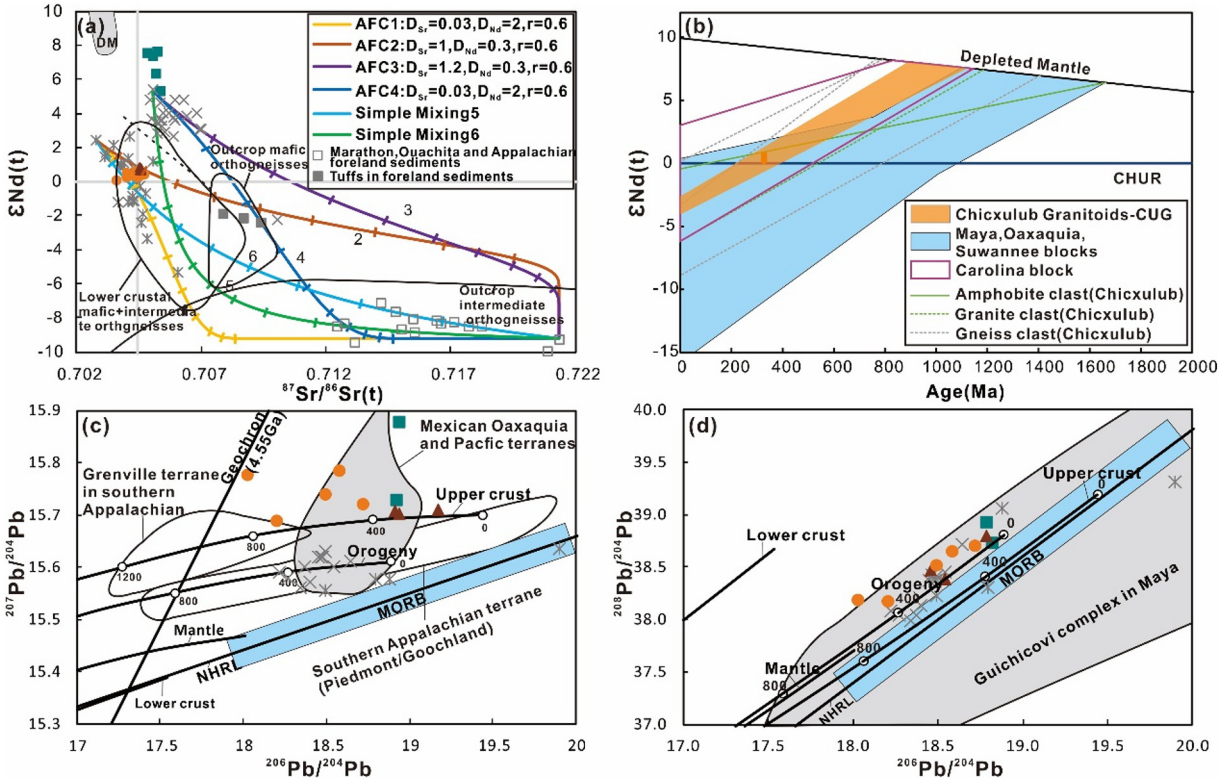

Fig. 12. Diagram of Sr–Nd–Pb isotopic features. (a). Regional Sr-Nd isotope data including Maya, Oaxaquia Suwannee and Carolina blocks, and the Late Paleozoic magmatic rocks, is from Heatherington et al. (2010); Keppie et al. (2012); Lopez and Cameron (1997); Ruiz et al. (1988b); Samson et al. (1995a) and Ruiz et al. (1988a) Sr-Nd isotopes for foreland sediments and tuffs from Marathon and Ouachita and Appalachian foreland sediments are similar in Nd isotopes (εNd(t) = −7–−10) (Gleason et al., 1995). Partition coefficients of Sr and Nd, and the AFC models are from DePaolo (1981b), the simple mixing model is from DePaolo and Wasserburg (1979). (b). Sr-Nd isotopes for the clasts (amphibole, granite and gneiss) in the Chicxulub impact crater are from Kettrup and Deutsch (2003). (c-d). Pb isotope data for the Grenville terrane in the southern Appalachian, the southern Appalachian terrane (Piedmont/Goochland), the Mexican Oaxaquia and Pacific terranes, and Guichicovi complex in Maya are from Keppie and Dallmeyer (1995) and Ruiz et al. (1999), the evolution curves of upper crust, lower crust, orogeny and mantle are from Zartman and Doe (1981). The NHRL (Northern Hemisphere reference line) is from Hart (1984). MORB (Mid–Ocean ridge basalt) region is from Zindler and Hart (1986). Data sources and symbols are the same as in Fig. 11.

mantle, which can generate granitic or rhyolitic, alkaline to ultrapotassic basaltic and MORB–like or OIB–like rocks, respectively (Davies and Blanckenburg, 1995; Kay and Kay, 1993). This type of magmatism tends to produce a linear magmatic zone because of rapid lateral slab breakoff, and relatively small volumes of melt (Davies and Blanckenburg, 1995; Samson et al., 1995a). When the slab breaks off, the relatively light subducted continent becomes buoyant, and this leads to a rapid rise in elevation. Consequently, there is an increase in the rate of deposition of clastic sediments especially on the foreland. A series of sedimentary records reveal that the rate of sediment deposition in the Ouachita foreland increased significantly to a maximum thickness of ~ 16,000 m during the Late Mississippian to the Middle Pennsylvanian (Shaulis et al., 2012), which is thicker than that in the Marathon and Sonora region (Morris, 1989; Poole et al., 2005). These sediments may have been derived from the southern Appalachian region (Shaulis et al., 2012), indicating a trend of rapid uplift, which was a knock–on effect coeval with the formation of the Chicxulub granitoids of this study. There are no Late Paleozoic detrital zircons in the Ouachita foreland (Gleason et al., 2007), which is consistent with there being little continental arc in the Carolina and Suwannee blocks during the assembly of Pangea (Mueller et al., 2014). In contrast, the Late Paleozoic zircons (~ 320 Ma) in the Marathon foreland may be derived from the Las Delicias arc or the Yucatán region (Gleason et al., 2007), and the detrital mica (^{40}Ar-^{39}Ar age of ~ 310 Ma) in the San Cayetano Formation in western Cuba may also be sourced from the Yucatan region (Hutson et al., 1998). However, according to model–A from Keppie and Keppie (2013) and Seton et al. (2012), the northern Maya block is more proximal to the Carolina and Suwannee block, whose similar basement attributes will be discussed in Section 5.5. Furthermore, the remnant of oceanic slab or crust is suggested in a density model obtained from gravity data across the Ouachita Mountains and the Gulf of Mexico (Mickus and Keller, 1992), supporting slab breakoff.

Slab breakoff often precedes the main phase of collision–driven compression. Its corresponding magmas are generated earlier than the termination of compressive deformation. Deformation in the Ouachita belt began in the Middle Mississipian and ended in the Late Pennsylvanian (Poole et al., 2005). Therefore, this timing supports the slab breakoff model rather than the thickened crust or mantle delamination model. The idea that the overriding continental crust thickens during this process has been verified by similar K–rich adakitic rocks in Tibet (Lee et al., 2007). The high Sr/Y and La_N/Yb_N ratios suggest that the lower crust in the Maya block underwent crustal thickening. However, the low content of garnet and very low content of rutile in residues do not favor a huge degree of crustal thickening (>60 km), which is more likely to occur in a post–collisional period. Thus, the slab breakoff model appears more likely than the thickened crust or mantle delamination model, as it is able to explain the relatively low degree of crustal thickening that happened in the pre–collision and syn–collision period, when the Rheic ocean subducted beneath Gondwana.

The felsite dykes in this study are concomitant magma derived from metasomatic mantle according to the aforementioned trace elements features. Their slightly positive $\varepsilon Nd_{(t)}$ and low $^{87}Sr/^{86}Sr_{initial}$ are indicative of a less evolved metasomatic mantle source (Lee et al., 2009). Thus, they may have formed by the heating from upwelling asthenosphere materials. The dolerite dykes possess features of the asthenospheric mantle, thus they are also consistent with a slab breakoff model.

5.5. Comparisons of Late Paleozoic magmatism in the Maya, Oaxaquia, Suwannee and Carolina blocks

5.5.1. The similarities and differences of magma sources and processes

The Maya, Oaxaquia, Carolina and Suwannee blocks are significant constituents of the Peri–Gondwanan realm, where Late Paleozoic magmatism mainly occurred during the assembly of Pangea. The specifics of the coeval magmatism in each of these blocks can help us understand the nature of the basement at each location as well as its tectonic evolution. The coeval magmatism on the Maya, Suwannee and Carolina blocks resulted in overlapping isotopic features according to Fig. 12 c, which suggests a collective juvenile source of Pan–African–aged materials (i.e. not Grenvillian–aged materials). We chose the least evolved Las Delicias arc in the Oaxaquia block and Alleghanian granite in the Carolina block as parental magma endmembers and the most evolved foreland sediments from the Marathon and Ouachita Orogen as evolved endmembers to ascertain the AFC processes by Sr-Nd isotopes. The modelling results are shown in Supplement 6.

5.5.1.1. Oaxaquia block. The Las Delicias region in Coahuila has outcrops of peperite, granites and dacite ash. Their lower Rb/Sr ratios (mostly <0.05), and typical arc features, such as negative anomalies in Nb and Ti, enrichments in LILE, and depletion in HREE (Fig. 8 b), point to a link with continental arc magmatism (Lopez and Cameron, 1997). The lower Rb/Sr and La/Yb ratios represent the absence of crust contamination processes, which may imply a thin crust (Lopez and Cameron, 1997). Their positive range of εNd (t) values (+2.7–5.45) and higher $^{87}Sr/^{86}Sr$ (t) ratios (0.7050–0.7070, 0.71) collectively indicate that their sources are slab–fluid metasomatic mantle materials, and AFC processes mainly appear as plagioclase fractional crystallization with minimal contamination from upper crustal materials. As the western part of the Marathon–Ouachita–Appalachian orogen, the Oaxaquia block contained only continental arc magmatic rocks during the convergence of Pangea (McKee et al., 1988, 1999; Ortega-Gutiérrez et al., 2018). These features suggest a continuous continental arc setting for the Oaxaquia block during the assembly of Pangea.

5.5.1.2. Suwannee block. Late Paleozoic magmatism is scarce in the Suwannee block, possibly because it is concealed by Mesozoic cover similar to the Maya block (Mueller et al., 2014). However, A–type granites related to post–collisional, lithospheric delamination events (Heatherington et al., 2010) were recovered in drill cores. They display high K_2O contents, high Rb/Sr ratios (Fig. 11 b, d), intermediate $^{87}Sr/^{86}Sr_{(300Ma)} = 0.70377$ (Fig. 12 a), T_{DM1} of 1.1–0.7 Ga and inherited zircon ages of 560 Ma and 1.2–1.0 Ga (Table. 2). All these features reveal that these granites were sourced from less evolved Pan–African crust. Moreover, high Y (22.8–46.8 ppm), Nb (22.3–68.9 ppm) and low Y/Nb (<1.2) are indicators for the involvement of asthenospheric mantle (Fig. 11 c, e, f) (Heatherington et al., 2010). According to AFC processes modelled by Sr-Nd isotopes, Suwannee granites have a high $^{87}Sr/^{86}Sr_{(300Ma)}$, indicative of contamination with upper crustal materials (Heatherington et al., 2010) (Fig. 12 a), meanwhile, they do show obvious contamination with upper crustal materials according to the Rb/Sr versus Rb/Ba diagram (Fig. 11 d).

5.5.1.3. Carolina block. The Carolina block hosts extensive Late Paleozoic magmatic rocks, especially Alleghanian granites, that are attributed to post–collisional or strike–slip tectonic environments (Heatherington et al., 2010; Mueller et al., 2014). Some of them are divided into A–type granites for their high Ga/Al ratios. Most of them are not related to continental arc rocks (Samson et al., 1995a; Speer and Hoff, 1997; Speer et al., 1994), and most of the Alleghanian granites are K–rich and show high Rb/Sr ratios and Nb + Y contents, which demonstrates more involvement of upper crustal and asthenospheric mantle materials. The Rb/Ba versus Rb/Sr diagram (Fig. 11 d), indicates that the parental magma of the Alleghanian granites from Carolina and/or Inner Piedmont involved more upper crustal materials (clay–rich sources) than the parental magma for the Chicxulub granitoids in this study. The negative Sr anomalies (Fig. 8 b) reveal that the parental magma of Alleghanian granites may have been affected by the fractional crystallization of plagioclase (Fig. 11 e, f). However, some Alleghanian granites show a trend of amphibolite fractional crystallization through low D_{Sr} and high D_{Nd} (DePaolo, 1981b) (Fig. 11 a), which may explain some positive Sr anomalies in Alleghanian granites. An alternative explanation is that amphibolite was part of the residue when the source melted. As for the source of Alleghanian granites in the Carolina block, they are more similar to source 1 (mafic metavolcanic arc rocks) because of their high contents of LILE.

In summary, the coeval granitoids in the Maya, Suwannee and Carolina blocks display similarities in their mineral assemblages, high K, Rb/Sr ratios and juvenile isotopic characteristics, which suggests that they may have been sourced from a similar juvenile lower crustal basement (Pan–African materials) (Heatherington et al., 1997; Keppie et al., 2011; Keppie et al., 2012; Samson et al., 1995a). It is possible that the Chicxulub granitoids are the western extension of the Alleghanian granites. The major divergences in trace elements such as Rb, Sr, Ba, Nb and Y are caused by different AFC processes such as the involvement of upper crustal or asthenospheric mantle materials and plagioclase or amphibole fractional crystallization. Magmatism in the Oaxaquia block, appears to have been sourced from less enriched continental lithospheric mantle (Lopez and Cameron, 1997).

5.5.2. The asynchronous magmatism along the convergent margin of Pangea

The supercontinent Pangea formed by asynchronous collision between Gondwana and Laurentia (Poole et al., 2005) during the Marathon–Ouachita–Appalachian orogeny. Deformation in three segments of the Marathon–Ouachita–Appalachian orogen began approximately in the Middle to Late Mississippian, and ended diachronously in the Early Permian in the Marathon region, the Late Pennsylvanian in the Ouachita Mountains, and the Middle Pennsylvanian in the southern Appalachian region (Dallmeyer et al., 1986; Poole et al., 2005; Sacks and Secor, 1990). Therefore, the convergence between Gondwana and Laurentia commenced simultaneously, but ended earlier in the east and later in the west (Poole et al., 2005). The Late Paleozoic magmatism in the Oaxaquia, Maya, Suwannee, and Carolina blocks occurred from west to east at 331–270 Ma (Lopez and Cameron, 1997), 326 ± 5 Ma (in this study), 296–295 Ma (Heatherington et al., 2010), and 335–285 Ma (Samson et al., 1995a; Winchester, 2013), respectively (Table 2). Magmatism roughly coincided with orogenic deformation periods, which hints at their evolutionary relationship in space and time. It

Table 2
Comparison of Late Paleozoic magmatic rocks in the Carolina, Suwannee, Maya and Oaxaquia blocks. These features are summarized from Heatherington et al. (2010); Lopez and Cameron (1997); Speer and Hoff (1997).

Magmatism	Age	Inherited zircons	Possible basement	εNd(t)	Inferred tectonic setting
Carolina	285–326 Ma	---	Pan–African	−6.2–2.67	Post–collisional
Suwannee	294–296 Ma	560 Ma/1100–1200 Ma	Pan–African or Grenvillian	−1–1.6	Post–collisional
Maya	326 ± 5.3 Ma	589 Ma/1100 Ma	Pan–African or Grenvillian	0.17–0.68	Pre– or syn–collisional to post–collisional
Oaxaquia	270–331 Ma	---	Grenvillian	−2.17–5.45	Continental arc

is plausible that magmatism ended earlier in the east and later in the west in the Marathon–Ouachita–Appalachian orogen.

To ascertain the continuity of delamination via related magmatism in the Marathon–Ouachita–Appalachian orogen, the ending time of continental arc magmatism in this orogeny is key evidence. As discussed above, although Alleghanian granites may have formed due to some early continental arc magmatism (east Blue Ridge) (Winchester, 2013), the major granites are from crustal sources which indicates that the continental arc setting ended early in the southern Appalachian region. Meanwhile, there are some continental arc rocks in the Maya block (such as tuffs and andesite) (Marton and Buffler, 1994), but synchronous Chicxulub granitoids represent the products of lower crustal melting. This indicates a transformation from pre–collisional to syn–collisional or post–collisional magmatism and a continuous delamination in the Marathon–Ouachita–Appalachian orogen from the Carolina block to the Maya block. The continuous continental arc magmatism in the Oaxaquia block suggests it did not undergo the delamination process; this finding may imply that there was an interruption of delamination between the Maya and Oaxaquia blocks.

5.5.3. Comparison of geodynamic mechanisms

With the closing of the Rheic ocean, heat from the upwelling asthenosphere during delamination may have acted as a driving force to generate the Alleghanian granites by melting Pan–African–aged lower crust in the Carolina and Suwannee blocks (Heatherington et al., 2010; Sacks and Secor, 1990; Speer and Hoff, 1997). In contrast to the Chicxulub granitoids and Alleghanian granites, Sr/Y and La/Yb ratios suggest that, there is no obvious evidence of crustal thickening in the Carolina and Suwannee blocks. Thus, these findings do not completely support the delamination of thickened crust and mantle throughout the Marathon–Ouachita–Appalachian orogen. Additionally, in the Oaxaquia block, the Late Paleozoic magmatism shows a continental arc setting from beginning to end. And the Chicxulub granitoids (non–continental arc rocks) in this study, plus some coeval continental arc rocks in boreholes in the Maya block (Marton and Buffler, 1994) and the presence of tuffs (continental arc type) with nearly similar ages in the Ouachita foreland (Loomis et al., 1994; Poole et al., 2005; Shaulis et al., 2012) are not consistent with a transpressional model. Therefore, the crust thickening model and transpressional model seem unable to completely explain this phenomenon across the whole region including the Carolina, Suwannee, Maya and Oaxaquia blocks. A different mechanism is required to explain the transformation mechanism from continental arc to syn–collisional or post–collisional magmatism.

Considering the approximate simultaneity of magmatism and metamorphism in these three blocks, and the effects of the slab breakoff model in the southern Appalachian region reported in previous studies (Nelson, 1992; Sacks and Secor, 1990; Samson et al., 1995a), a tearing slab breakoff model was put forward (Fig. 13) to explain the differences and similarities of magmatism and tectonism over the whole region during the Marathon–Ouachita–Appalachian orogeny. Slab breakoff would commence in a certain place and propagate along strike (Yoshioka and Wortel, 1995). The detached slab would give an additional drag force on the adjacent undetached slab, and promote the lateral propagation (Wortel and Spakman, 1992). Plausibly, the depth of detachment will migrate into a deeper level owing to the resultant force of both the lower slab and the neighboring detached slab. On the other hand, the rate of convergence could affect the depth of breakoff (Davies and Blanckenburg, 1995). This model can explain some major features of the magmatism along the Marathon–Ouachita–Appalachian orogen (Fig. 1 and Fig. 13 a, b):

(1) Syn–collisional or post–collisional magmatism and very minor pre–collisional magmatism occurred in the east of the Marathon–Ouachita–Appalachian orogen (Carolina block), in contrast, abundant continental arc magmatic rocks were emplaced in the west (Oaxaquia block) (Dickinson, 2009; Dickinson and Lawton, 2001). This style of magmatism can be attributed to the depth of the breakoff site. According to the timing of magmatism, slab breakoff commenced in the Carolina block at a relatively shallow depth so that there are no metasomatic mantle materials to facilitate the formation of continental arc magmatism (Fig. 12 c, d). The slab gradually detaches deeper in the Maya block, causing the melting of metasomatic mantle materials above the detaching site to generate both syn– or post–collisional magma and continental arc magma (Fig. 13 c, e). Due to a deeper breakoff site or no slab break off in the west, only continental arc magmas were generated in the Oaxaquia block (Fig. 13 c, e).
(2) All the Late Paleozoic magmatism in the three blocks (Carolina, Suwannee and Maya) is dispersed along the Marathon–Ouachita–Appalachian orogen. The volume, east–to–west along strike and gradual age changes of Late Paleozoic magmatism along the Peri–Gondwanan realm resemble magmatism caused by the tearing slab breakoff model in Tibet and the Alps (Davies and Blanckenburg, 1995; Zhang et al., 2014) because slab breakoff leads to magmatism distributed linearly with relatively smaller volumes than those generated by thickened crust delamination (Davies and Blanckenburg, 1995; Samson et al., 1995a). The Y/Nb ratios of Alleghanian granites in the Suwannee block are lower than that of Alleghanian granites in the Carolina block, while the 10000*(Ga/Al) values are higher (Heatherington et al., 2010). The A-type Alleghanian granites in the Suwannee block were likely caused by the direction of upwelling asthenospheric mantle in the right of Fig. 13 f, which is quite similar to the popular slab rollback model for the formation of A-type granites (Li et al., 2014). Therefore, the timing of the granites formation in the Suwannne block and Carolina block may be a bit different. More importantly, the occurrence of the K–rich adakitic Chicxulub granitoids further supports the slab breakoff model.
(3) The contributions of upper crustal and asthenospheric mantle are divergent in granitoids in the Maya block and Carolina block, which could also be related to the depth of the slab breakoff site. Different contributing portions from mantle and upper crustal materials involved in the formation of these Late Paleozoic magmatic rocks in three blocks can be observed. If the asthenospheric mantle upwells at a shallow site (e.g. shallower than 50 km) (Davies and Blanckenburg, 1995), decompression will cause it to melt, and more characteristics of asthenospheric mantle will be imparted into crustal melts such as the Alleghanian granites (high Nb and Y content). If such asthenospheric mantle upwells at a deeper site (e.g. deeper than 50 km), such as in the Maya block, the asthenosphere would not melt and, instead, would merely heat the overlying metasomatic mantle and crust that has been thickened. Therefore, less asthenospheric materials would become involved in the resulting magma.

6. Conclusions

(1) We report the first U-Pb age of 326 ± 5 Ma from zircons in the Chicxulub granitoids from the peak ring of the Chicxulub impact crater. This age contrasts with the dominant Pan-African-aged zircon population revovered from K-Pg boundary sections and other Chicxulub-related deposits, in which zircons with carboniferous ages are rare. Meanwhile, the Chicxulub granitoids represent the extensional magmatic expressions of Alleghanian granites (335–285 Ma) during the assembly of Pangea.
(2) The Late Paleozoic Chicxulub granitoids are K–rich adakitic rocks derived from the melting of thickened crust with a residue of garnet–bearing amphibolite or garnet–bearing granulite.

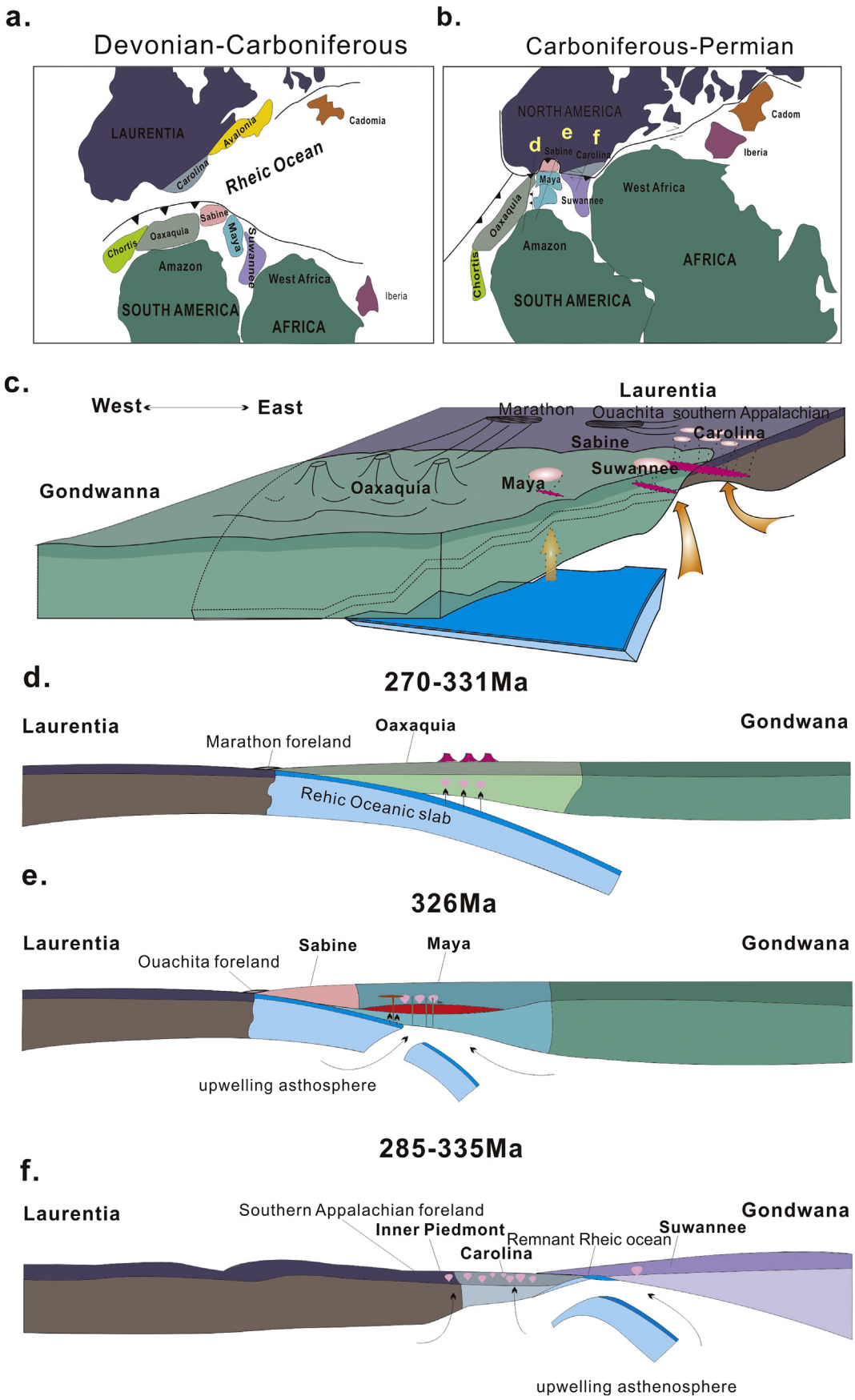

Fig. 13. Schematic models for Late Paleozoic magmatic activities on the Carolina, Suwannee, Maya and Oaxaquia blocks, diagram a, b are modified from Mueller et al. (2014), Weber et al. (2008) and Dickinson (2009), diagram d is modified from Sacks and Secor (1990).

Thickened crust was heated by upwelling asthenospheric mantle, which resulted from slab breakoff. These processes also caused metasomatic mantle melting, which generated the intrusions of shoshonitic felsite. Dolerite dykes represent asthenospheric mantle derived melts that may be related to this geodynamic process or a later Mesozoic episode.

(3) Hf model ages in zircons, Nd model ages and equilibrium melting models of trace elements reveal that the Chicxulub granitoids were sourced from a juvenile lower crust (Pan–African Orogeny materials) that was similar to the basement of the Carolina block. The northern Maya block (the site of the Chicxulub impact crater) was proximal to the Carolina block and Suwannee blocks during the assembly of Pangea. Coeval magmatic rocks on the Suwannee and the Carolina blocks also have similar sources, but involve more upper crustal and asthenospheric mantle materials.

(4) The similarities and differences of magmatic expressions in the Oaxaquia, Maya, Suwannee and Carolina blocks are consistent with asynchronous convergence and a tearing slab breakoff that propagated from east to west during the formation of Pangea. The depth of slab breakoff is responsible for the divergence in magma types in the Oaxaquia, Maya, Suwannee and Carolina blocks, that occurred during the assembly of Pangea.

Supplementary data to this article can be found online at https://doi.org/10.1016/j.gr.2019.12.003.

Declaration of competing interest

The authors declare that they have no known competing financial interests or personal relationships that could have appeared to influence the work reported in this paper.

Acknowledgments

This study was funded by the National Natural Science Foundation of China (41772050, 41830214, 41773061), MOST Special Fund from the State Key Laboratory of Geological Processes and Mineral Resources, China University of Geosciences (MSFGPMR05) and the Science and Technology Development Fund (FDCT) of Macau (Grant No. 121/2017/A3). This research used samples and data provided by the IODP and recovered in the context of Expedition 364, which was funded by the IODP with co–funding from the ICDP. Expedition 364 was implemented by ECORD, with contributions and logistical support from the Yucatán state government and Universidad Nacional Autonoma de Mexico. SPSG supported by NSF–OCE–1737351. JVM by NERC grant NE/P005217/1. AW was supported by NSF–OCE–1737087. The Vrije Universiteit Brussel group is supported by Research Foundation Flanders (FWO) and BELSPO; PK is an FWO PhD fellow. This research used data acquired at the MARUM–Center for Marine Environmental Sciences, University of Bremen, Germany.

References

Abramov, O., Kring, D.A., 2007. Numerical modeling of impact-induced hydrothermal activity at the Chicxulub crater. Meteorit. Planet. Sci. 42, 93–112.

Baker, J., Peate, D., Waight, T., Meyzen, C., 2004. Pb isotopic analysis of standards and samples using a 207Pb–204Pb double spike and thallium to correct for mass bias with a double-focusing MC-ICP-MS. Chem. Geol. 211, 275–303.

Castillo, P.R., Janney, P.E., Solidum, R.U., 1999. Petrology and geochemistry of Camiguin Island, southern Philippines: insights to the source of adakites and other lavas in a complex arc setting. Contrib. Mineral. Petrol. 134, 33–51.

Centeno-García, E., 2016. Mesozoic tectono-magmatic evolution of Mexico: an overview. Ore Geol. Rev. 81, 1035–1052.

Chung, S.L., Liu, D., Ji, J., Chu, M.F., Lee, H.Y., Wen, D.J., Lo, C.H., Lee, T.Y., Qian, Q., Zhang, Q., 2003. Adakites from continental collision zones: Melting of thickened lower crust beneath southern Tibet. Geology 31, 1021–1024.

Clift, P.D., Heinrich, P., Dunn, D., Jacobus, A., Blusztajn, J., 2017. The Sabine block, Gulf of Mexico: Promontory on the north American margin? Geology 46, 15–18.

Condie, K.C., 1993. Chemical composition and evolution of the upper continental crust: contrasting results from surface samples and shales. Chem. Geol. 104, 1–37.

Dallmeyer, R.D., 1989. Contrasting accreted terranes in the southern Appalachian Orogen, basement beneath the Atlantic and Gulf Coastal Plains, and West African orogens. Precambrian Res. 42, 387–409.

Dallmeyer, R.D., Wright, J.E., Secor, D.T., Snoke, A.W., 1986. Character of the Alleghanian orogeny in the southern Appalachians: Part II. Geochronological constraints on the tectonothermal evolution of the eastern Piedmont in South Carolina. GSA Bull. 97, 1329–1344.

Davies, J.H., Blanckenburg, F., 1995. Slab breakoff: a model of lithosphere detachment and its test in the magmatism and deformation of collisional orogens. Earth Planet. Sci. Lett. 129, 85–102.

Defant, M.J., Drummond, M.S., 1990. Derivation of some modern arc magmas by melting of young subducted lithosphere. Nature 347, 662–665.

Dennis, A.J., Shervais, J.W., Mauldin, J., Maher Jr., H.D., Wright, J.E., 2004. Petrology and geochemistry of Neoproterozoic volcanic arc terranes beneath the Atlantic Coastal Plain, Savannah River Site, South Carolina. GSA Bull. 116, 572–593.

Depaolo, D.J., 1981a. A neodymium and strontium isotopic study of the Mesozoic calc-alkaline granitic batholiths of the Sierra Nevada and Peninsular Ranges, California. Journal of Geophysical Research Solid Earth 86, 10470–10488.

DePaolo, D.J., 1981b. Trace element and isotopic effects of combined wallrock assimilation and fractional crystallization. Earth Planet. Sci. Lett. 53, 189–202.

DePaolo, D.J., Wasserburg, G.J., 1979. Petrogenetic mixing models and Nd-Sr isotopic patterns. Geochim. Cosmochim. Acta 43, 615–627.

Dickinson, W.R., 2009. The Gulf of Mexico and the southern margin of Laurentia. Geology 37, 479–480.

Dickinson, W.R., Lawton, T.F., 2001. Carboniferous to cretaceous assembly and fragmentation of Mexico. Geol. Soc. Am. Bull. 113, 1142–1160.

Farmer, G.L., DePaolo, D.J., 1987. Nd and Sr isotope study of hydrothermally altered granite at San Manuel, Arizona; implications for element migration paths during the formation of porphyry copper ore deposits. Econ. Geol. 82, 1142–1151.

Fullagar, P.D., 2002. Evidence for early Mesoproterozoic (and older?) crust in the Southern and Central Appalachians of North America. Gondwana Res. 5, 197–203.

Gao, S., Rudnick, R.L., Yuan, H.-L., Liu, X.-M., Liu, Y.-S., Xu, W.-L., Ling, W.-L., Ayers, J., Wang, X.-C., Wang, Q.-H., 2004. Recycling lower continental crust in the North China craton. Nature 432, 892–897.

Gleason, J.D., Patchett, P.J., Dickinson, W.R., Ruiz, J., 1995. Nd isotopic constraints on sediment sources of the Ouachita-Marathon fold belt. GSA Bull. 107, 1192–1210.

Gleason, J.D., Gehrels, G.E., Dickinson, W.R., Patchett, P.J., Kring, D.A., 2007. Laurentian sources for detrital zircon grains in turbidite and deltaic sandstones of the Pennsylvanian Haymond Formation, Marathon Assemblage, West Texas, U.S.A. J. Sediment. Res. 77, 888–900.

Govindaraju, K., 1994. Compilation of working values and sample description for 383 geostandards. Geostand. Newslett. 18, 1–158.

Gulick, S., Morgan, J., Mellett, C.L., Chenot, E., Christeson, G.L., Claeys, P., Cockell, C.S., Coolen, M.J.L., Ferrière, L., Gebhardt, C., Goto, K., Green, S., Jones, H., Kring, D.A., Lofi, J., Lowery, C.M., Ocampo-Torres, R., Perez-Cruz, L., Pickersgill, A.E., Poelchau, M., Rae, A.S.P., Rasmussen, C., Rebolledo-Vieyra, M., Riller, U., Sato, H., Smit, J., Tikoo, S.M., Tomioka, N., Urrutia-Fucugauchi, J., Whalen, M.T., Wittmann, A., Xiao, L., Yamaguchi, K.E., Zylberman, W., Collins, G.S., Bralower, T.J., 2017. Expedition 364 preliminary report: Chicxulub: drilling the K-Pg impact crater.

Gulick, S.P.S., Barton, P.J., Christeson, G.L., Morgan, J.V., McDonald, M., Mendoza-Cervantes, K., Pearson, Z.F., Surendra, A., Urrutia-Fucugauchi, J., Vermeesch, P.M., Warner, M.R., 2008. Importance of pre-impact crustal structure for the asymmetry of the Chicxulub impact crater. Nat. Geosci. 1, 131.

Hardarson, B.S., Fitton, J.G., 1991. Increased mantle melting beneath Snaefellsjökull volcano during Late Pleistocene deglaciation. Nature 353, 62.

Hart, S.R., 1984. A large-scale isotope anomaly in the Southern Hemisphere mantle. Nature 309, 753–757.

Heatherington, A., Mueller, P., Nutman, A., 1996. Neoproterozoic magmatism in the Suwannee Terrane: Implications for terrane correlation. In: Nance, R.D. and Thompson, M.D., Avalonian and related peri-Gondwanan terranes of the Circum-North Atlantic, Geological Society of America Special Paper 304, 257–268.

Heatherington, A.L., Mueller, P.A., 1999. Lithospheric sources of North Florida, USA tholeiites and implications for the origin of the Suwannee terrane. Lithos 46, 215–233.

Heatherington, A.L., Mueller, P.A., 2003. Mesozoic igneous activity in the Suwannee Terrane, Southeastern USA: Petrogenesis and Gondwanan Affinities. Gondwana Res. 6, 296–311.

Heatherington, A.L., Mueller, P.A., Randazzo, A., Jones, D., 1997. Geochemistry and Origin of Florida Crustal Basement Terranes. Gainesville, University Press of Florida, The geology of Florida, pp. 27–37.

Heatherington, A.L., Mueller, P.A., Wooden, J.L., 2010. Alleghanian plutonism in the Suwannee terrane, USA: implications for late Paleozoic tectonic models. In: Tollo, R.P., Bartholomew, M.J., Hibbard, J.P., Karabinos, P.M. (Eds.), From Rodinia to Pangea: The Lithotectonic Record of the Appalachian Region. Geological Society of America, pp. 607–620.

Hecht, L., Wittmann, A., Schmitt, R.-T., Stöffler, D., 2004. Composition of impact melt particles and the effects of post-impact alteration in suevitic rocks at the Yaxcopoil-1 drill core, Chicxulub crater, Mexico. Meteorit. Planet. Sci. 39, 1169–1186.

Helvaci, C., Griffin, W.L., 1983. Metamorphic feldspathization of metavolcanics and granitoids, Avnik area, Turkey. Contrib. Mineral. Petrol. 83, 309–319.

Hibbard, J., Staal, C., Rankin, D., Williams, H., 2006. Lithotectonic map of the Appalachian orogen (north), Canada-United States of America. Bulletin of the Geological Survey of Canada map 2096A, 2.

Hibbard, J.P., Stoddard, E.F., Secor, D.T., Dennis, A.J., 2002. The Carolina Zone: overview of Neoproterozoic to Early Paleozoic peri-Gondwanan terranes along the eastern Flank of the southern Appalachians. Earth Sci. Rev. 57, 299–339.
Hibbard, J.P., van Staal, C.R., Miller, B.V., 2007. Links among Carolinia, Avalonia, and Ganderia in the Appalachian peri-Gondwanan realm. Geol. Soc. Am. Spec. Pap. 433, 291–311.
Hughes, C.J., 1972. Spilites, keratophyres, and the igneous spectrum. Geol. Mag. 109, 513–527.
Hutson, F., Mann, P., Renne, P., 1998. 40Ar/39Ar dating of single muscovite grains in Jurassic siliciclastic rocks (San Cayetano Formation): constraints on the paleoposition of western Cuba. Geology 26, 83–86.
Imai, N., Terashima, S., Itoh, S., Ando, A., 1995. Compilation of analytical data for minor and trace elements in seventeen GSJ geochemical reference samples, "igneous rock series". Geostand. Newslett. 19, 135–213.
Jackson, S.E., Pearson, N.J., Griffin, W.L., Belousova, E.A., 2004. The application of laser ablation-inductively coupled plasma-mass spectrometry to in situ U–Pb zircon geochronology. Chem. Geol. 211, 47–69.
Kamo, S.L., Krogh, T.E., 1995. Chicxulub crater source for shocked zircon crystals from the Cretaceous-Tertiary boundary layer, Saskatchewan: evidence from new U-Pb data. Geology 23, 281–284.
Kamo, S.L., Lana, C., Morgan, J.V., 2011. U–Pb ages of shocked zircon grains link distal K–Pg boundary sites in Spain and Italy with the Chicxulub impact. Earth Planet. Sci. Lett. 310, 401–408.
Kay, R.W., Kay, S.M., 1993. Delamination and delamination magmatism. Tectonophys 219, 177–189.
Keppie, D.F., Keppie, J.D., 2013. The Yucatan, a Laurentian or Gondwanan fragment? Geophysical and palinspastic constraints. Int. J. Earth Sci. 103, 1501–1512.
Keppie, J.D., Dallmeyer, R.D., 1995. Late Paleozoic collision, delamination, short-lived magmatism, and rapid denudation in the Meguma Terrane (Nova Scotia, Canada): constraints from 40Ar/39Ar isotopic data. Can. J. Earth Sci. 32, 644–659.
Keppie, J.D., Ortega-Gutiérrez, F., 2010. 1.3–0.9Ga Oaxaquia (Mexico): Remnant of an arc/backarc on the northern margin of Amazonia. Journal of South American Earth Sciences 29, 21–27.
Keppie, J.D., Dostal, J., Nance, R.D., Miller, B.V., Ortegarivera, A., Lee, J.K.W., 2006. Circa 546 Ma plume-related dykes in the ~1 Ga Novillo Gneiss (east-central Mexico): evidence for the initial separation of Avalonia. Precambrian Res. 147, 342–353.
Keppie, J.D., Dostal, J., Norman, M., Urrutia-Fucugauchi, J., Grajales-Nishimura, M., 2011. Study of melt and a clast of 546 Ma magmatic arc rocks in the 65 Ma Chicxulub bolide breccia, northern Maya block, Mexico: western limit of Ediacaran arc peripheral to northern Gondwana. Int. Geol. Rev. 53, 1180–1193.
Keppie, J.D., Murphy, J.B., Nance, R.D., Dostal, J., 2012. Mesoproterozoic Oaxaquia-type basement in peri-Gondwanan terranes of Mexico, the Appalachians, and Europe: TDM age constraints on extent and significance. Int. Geol. Rev. 54, 313–324.
Kettrup, B., Deutsch, A., 2003. Geochemical variability of the Yucatàn basement: constraints from crystalline clasts in Chicxulub impactites. Meteorit. Planet. Sci. 38, 1079–1092.
Kettrup, B., Deutsch, A., Ostermann, M., Agrinier, P., 2000. Chicxulub impactites: Geochemical clues to the precursor rocks. Meteorit. Planet. Sci. 35, 1229–1238.
Kring, D.A., 2005. Hypervelocity collisions into continental crust composed of sediments and an underlying crystalline basement: comparing the Ries (~24 km) and Chicxulub (~180 km) impact craters. Chemie der Erde - Geochemistry - Interdisciplinary Journal for Chemical Problems of the Geosciences and Geoecology 65, 1–46.
Kring, D.A., Durda, D.D., 2002. Trajectories and distribution of material ejected from the Chicxulub impact crater: Implications for postimpact wildfires. Journal of Geophysical Research Planets 107 (6), 1–22.
Kring, D.A., Hörz, F., Zurcher, L., Fucugauchi, J.U., 2004. Impact lithologies and their emplacement in the Chicxulub impact crater: initial results from the Chicxulub Scientific Drilling Project, Yaxcopoil, Mexico. Meteorit. Planet. Sci. 39, 879–897.
Krogh, T.E., Kamo, S.L., Bohor, B.F., 1993a. Fingerprinting the K/T impact site and determining the time of impact by U Pb dating of single shocked zircons from distal ejecta. Earth & Planetary Science Letters 119, 425–429.
Krogh, T.E., Kamo, S.L., Sharpton, V.L., Marin, L.E., Hildebrands, A.R., 1993b. U/Pb ages of single shocked zircons linking distal K/T ejecta to the Chicxulub crater. Nature 366, 731–734.
Large, R.R., Gemmell, J.B., Paulick, H., Huston, D.L., 2001. The alteration box plot: a simple approach to understanding the relationship between alteration mineralogy and lithogeochemistry associated with volcanic-hosted massive sulfide deposits. Econ. Geol. 96, 957–971.
Lee, H.Y., Chung, S.-L., Wang, Y., Zhu, D.-C., Yang, J.-H., Song, B., Liu, D.Y., Wu, F.-Y., 2007. Age, petrogenesis and geological significance of the Linzizong volcanic successions in the Linzhou basin, southern Tibet: evidence from zircon U-Pb dates and Hf isotopes. Acta Petrol. Sin. 23, 493–500.
Lee, H.Y., Chung, S.L., Lo, C.H., Ji, J., Lee, T.Y., Qian, Q., Zhang, Q., 2009. Eocene Neotethyan slab breakoff in southern Tibet inferred from the Linzizong volcanic record. Tectonophysics 477, 20–35.
Li, Z., Qiu, J.-S., Yang, X.-M., 2014. A review of the geochronology and geochemistry of Late Yanshanian (Cretaceous) plutons along the Fujian coastal area of southeastern China: Implications for magma evolution related to slab break-off and rollback in the Cretaceous. Earth Sci. Rev. 128, 232–248.
Liew, T.C., Hofmann, A.W., 1988. Precambrian crustal components, plutonic associations, plate environment of the Hercynian Fold Belt of central Europe: indications from a Nd and Sr isotopic study. Contrib. Mineral. Petrol. 98, 129–138.
Liu, Y., Gao, S., Yuan, H., Zhou, L., Liu, X., Wang, X., Hu, Z., Wang, L., 2004. U–Pb zircon ages and Nd, Sr, and Pb isotopes of lower crustal xenoliths from North China Craton: insights on evolution of lower continental crust. Chem. Geol. 211, 87–109.
Liu, Y., Gao, S., Hu, Z., Gao, C., Zong, K., Wang, D., 2010. Continental and oceanic crust recycling-induced melt–peridotite interactions in the Trans-North China Orogen: U–Pb dating, Hf isotopes and trace elements in zircons from mantle xenoliths. J. Petrol. 51, 537–571.
Loomis, J., Weaver, B., Blatt, H., 1994. Geochemistry of Mississippian tuffs from the Ouachita Mountains, and implications for the tectonics of the Ouachita orogen, Oklahoma and Arkansas. Geol. Soc. Am. Bull. 106, 1158–1171.
Lopez, R., Cameron, K.L., 1997. High-Mg andesites from the Gila Bend Mountains, southwestern Arizona: evidence for hydrous melting of lithosphere during Miocene extension. Geol. Soc. Am. Bull. 109, 900–914.
Ludwig, K.R., 2003. Isoplot 3.00: a geochronological toolkit for Microsoft Excel. Berkeley. Geochronol. Cent. Spec. Publ. 3, 1–70.
Ma, Q., Zheng, J.P., Xu, Y.G., Griffin, W.L., Zhang, R.S., 2015. Are continental "adakites" derived from thickened or foundered lower crust? Earth & Planetary Science Letters 419, 125–133.
Macpherson, C.G., Dreher, S.T., Thirlwall, M.F., 2006. Adakites without slab melting: High pressure differentiation of island arc magma, Mindanao, the Philippines. Earth Planet. Sci. Lett. 243, 581–593.
Manikyamba, C., Kerrich, R., Khanna, T.C., Satyanarayanan, M., Krishna, A.K., 2009. Enriched and depleted arc basalts, with Mg-andesites and adakites: a potential paired arc–back-arc of the 2.6Ga Hutti greenstone terrane, India. Geochim. Cosmochim. Acta 73, 1711–1736.
Martens, U., Weber, B., Valencia, V.A., 2010. U/Pb geochronology of Devonian and older Paleozoic beds in the southeastern Maya block, Central America: its affinity with peri-Gondwanan terranes. GSA Bull. 122, 815–829.
Martin, H., Smithies, R.H., Rapp, R., Moyen, J.F., Champion, D., 2005. An overview of adakite, tonalite–trondhjemite–granodiorite (TTG), and sanukitoid: relationships and some implications for crustal evolution. Lithos 79, 1–24.
Marton, G., Buffler, R.T., 1994. Jurassic reconstruction of the Gulf of Mexico Basin. Int. Geol. Rev. 36, 545–586.
McCulloch, M.T., Gamble, J.A., 1991. Geochemical and geodynamical constraints on subduction zone magmatism. Earth Planet. Sci. Lett. 102, 358–374.
McKee, J.W., Jones, N.W., Anderson, T.H., 1988. Las Delicias basin: a record of late Paleozoic arc volcanism in northeastern Mexico. Geology 16, 37–40.
McKee, J.W., Jones, N.W., Anderson, T.H., 1999. Late Paleozoic and Early Mesozoic History of the Las Delicias Terrane. Mexico. Special Paper of the Geological Society of America, Coahuila, pp. 161–190.
Mickus, K.L., Keller, G.R., 1992. Lithospheric structure of the south-central United States. Geology 20, 335–338.
Middelburg, J.J., van der Weijden, C.H., Woittiez, J.R.W., 1988. Chemical processes affecting the mobility of major, minor and trace elements during weathering of granitic rocks. Chem. Geol. 68, 253–273.
Morgan, J.V., Gulick, S.P.S., Bralower, T.J., Carter, G., Chenot, É., Christeson, G.L., Claeys, P.F., Cockell, C.S., Collins, G.S., Coolen, M., Ferrière, L., Gebhardt, C., Goto, K., Jones, H., Kring, D.A., Lofi, J., Lowery, C., Mellett, C., Ocampo-Torres, R., Osinski, G.R., Perez-Cruz, L.L., Pickersgill, A., Poelchau, M., Rae, A., Rasmussen, C., Rebolledo-Vieyra, M., Riller, U.P., Sato, H., Schmitt, D.R., Smit, J., Tikoo, S., Tomioka, N., Urrutia Fucugauchi, J., Whalen, M.T., Wittmann, A., Xiao, L., Yamaguchi, K.E., Zylberman, W., 2016. The formation of peak rings in large impact craters. Science 354, 878–882.
Morris, R.C., 1989. Stratigraphy and sedimentary history of post-Arkansas Novaculite Carboniferous rocks of the Ouachita Mountain, the Appalachian-Ouachita Orogen in the United States. Geological Society of America. Geology of North America 2, 591–602.
Moyen, J.-F., 2009. High Sr/Y and La/Yb ratios: the meaning of the "adakitic signature". Lithos 112, 556–574.
Mueller, P.A., Heatherington, A.L., Wooden, J.L., Shuster, R.D., Nutman, A.P., Williams, I.S., 1994. Precambrian zircons from the Florida basement: a Gondwanan connection. Geology 22, 119–122.
Mueller, P.A., Heatherington, A.L., Foster, D.A., Thomas, W.A., Wooden, J.L., 2014. The Suwannee suture: significance for Gondwana-Laurentia terrane transfer and formation of Pangaea. Gondwana Res. 26, 365–373.
Murphy, J.B., Pisarevsky, S.A., Nance, R.D., Keppie, J.D., 2004. Neoproterozoic—Early Paleozoic evolution of peri-Gondwanan terranes: implications for Laurentia-Gondwana connections. Int. J. Earth Sci. 93, 659–682.
Nelson, K.D., 1992. Are crustal thickness variations in old mountain belts like the Appalachians a consequence of lithospheric delamination? Geology 20, 498–502.
Ortega-Gutierrez, F., Ruiz, J., Centeno-Garcia, E., 1995. Oaxaquia, a Proterozoic microcontinent accreted to North America during the late Paleozoic. Geology 23, 1127–1130.
Ortega-Gutiérrez, F., Elías-Herrera, M., Morán-Zenteno, D.J., Solari, L., Weber, B., Luna-González, L., 2018. The pre-Mesozoic metamorphic basement of Mexico, 1.5 billion years of crustal evolution. Earth Sci. Rev. 183, 2–37.
Pearce, J.A., Peate, D.W., 1995. Tectonic implications of the composition of volcanic ARC magmas. Annu. Rev. Earth Planet. Sci. 23, 251–285.
Petford, N., Gallagher, K., 2001. Partial melting of mafic (amphibolitic) lower crust by periodic influx of basaltic magma. Earth Planet. Sci. Lett. 193, 483–499.
Pettingill, H.S., Sinha, A.K., Tatsumoto, M., 1984. Age and origin of anorthosites, charnockites, and granulites in the Central Virginia Blue Ridge: Nd and Sr isotopic evidence. Contrib. Mineral. Petrol. 85, 279–291.
Pollock, J., Hibbard, J., Sylvester, P., 2010. Depositional and tectonic setting of the Neoproterozoic–early Paleozoic rocks of the Virgilina sequence and Albemarle Group, North Carolina. Memoir of the Geological Society of America 206, 739.
Pollock, J., Hibbard, J., Staal, C., 2012. A paleogeographical review of peri-Gondwanan terranes of the Appalachian orogen. Can. J. Earth Sci. 49 (1), 259–288.
Pollock, J.C., Hibbard, J.P., 2010. Geochemistry and tectonic significance of the Stony Mountain gabbro, North Carolina: implications for the Early Paleozoic evolution of Carolinia. Gondwana Res. 17, 500–515.

Pollock, J.C., Hibbard, J.P., van Staal, C.R., 2011. A paleogeographical review of the peri-Gondwanan realm of the Appalachian orogen. Can. J. Earth Sci. 49, 259–288.
Poole, F.G., Perry, W.J., Madrid, R.J., Amaya-Martínez, R., 2005. Tectonic synthesis of the Ouachita-Marathon-Sonora orogenic margin of southern Laurentia: Stratigraphic and structural implications for timing of deformational events and plate-tectonic model. Geol. Soc. Am. Spec. Pap. 393, 543–596.
Qian, Q., Hermann, J.R., 2013. Partial melting of lower crust at 10-15 kbar:constraints on adakite and TTG formation. Contributions to Mineralogy & Petrology 165, 1195–1224.
Rapp, R., Shimizu, N., 2002. Experimental constraints on the origin of potassium-rich adakites in eastern China. Acta Petrol. Sinica 18, 293–311.
Rapp, R.P., Shimizu, N., Norman, M.D., Applegate, G.S., 1999. Reaction between slab-derived melts and peridotite in the mantle wedge: experimental constraints at 3.8 GPa. Chem. Geol. 160, 335–356.
Rasmussen, C., Stockli, D.F., Ross, C.H., Pickersgill, A., Gulick, S.P., Schmieder, M., Christeson, G.L., Wittmann, A., Kring, D.A., Morgan, J.V., 2019. U-Pb memory behavior in Chicxulub's peak ring — applying U-Pb depth profiling to shocked zircon. Chem. Geol. 525, 356–367.
Riller, U., Poelchau, M.H., Rae, A.S.P., Schulte, F.M., Collins, G.S., Melosh, H.J., Grieve, R.A.F., Morgan, J.V., Gulick, S.P.S.D., Lofi, J., Diaw, A., McCall, N., Kring, D.A., Iodp–Icdp Expedition 364 Science Party, 2018. Rock fluidization during peak-ring formation of large impact structures. Nature 562, 511–518. https://doi.org/10.1038/s41586-018-0607-z.
Rosales-Lagarde, L., Centeno-GarcãA, E., Dostal, J., Sour-Tovar, F., Ochoa-Camarillo, H., Quiroz-Barroso, S., 2005. The Tuzancoa Formation: evidence of an early Permian Submarine Continental Arc in East-Central Mexico. Int. Geol. Rev. 47, 901–919.
Ross, C.H., Stockli, D.F., Rasmussen, C., Gulick, S.P.S., de Graaff, S.J., Claeys, P., Zhao, J., Xiao, L., Pickersgill, A.E., Schmieder, M., Kring, D.A., Wittmann, A., Morgan, J.V., Party, I.S., 2019. Zircon U-Pb geochronology and trace elements of the Chicxulub impact structure basement, large meteorite impacts and planetary evolution VI. Lunar and Planetary Institute, Houston, p. Abstract #5120.
Ruiz, J., Patchett, P.J., Arculus, R.J., 1988a. Nd-Sr isotope composition of lower crustal xenoliths — evidence for the origin of mid-tertiary felsic volcanics in Mexico. Contrib. Mineral. Petrol. 99, 36–43.
Ruiz, J., Patchett, P.J., Ortegagutierrez, F., 1988b. Proterozoic and Phanerozoic basement terranes of Mexico from Nd isotopic studies. Geol. Soc. Am. Bull. 100, 274–281.
Ruiz, J., Tosdal, R.M., Restrepo, P.A., Murillo-Muñetón, G., 1999. Pb isotope evidence for Colombia-southern México connections in the Proterozoic Laurentia-Gondwana connections before Pangea. Special Papers-Geological Society of America 336, 183–198.
Sacks, P.E., Secor, D.T., 1990. Delamination in collisional orogens. Geology; (USA) 18 (10), 999–1002.
Samson, S.D., Coler, D.G., Speer, J.A., 1995a. Geochemical and Nd Sr Pb isotopic composition of Alleghanian granites of the southern Appalachians: origin, tectonic setting, and source characterization. Earth & Planetary Science Letters 134, 359–376.
Samson, S.D., Hibbard, J.P., Wortman, G.L., 1995b. Nd isotopic evidence for juvenile crust in the Carolina terrane, southern Appalachians. Contributions to Mineralogy & Petrology 121, 171–184.
Saunders, C., Tuach, J., 1988. K-Feldspathization, Albitization and Gold Mineralization in Granitoid Rocks: The Rattling Brook Alteration System, Western White Bay, Newfoundland. Newfoundland Department of Mines and Energy, Mineral Development Division, Report, pp. 307–317.
Schaaf, P., Weber, B., Weis, P., Gross, A., Köhler, H., Ortega-Gutiérrez, F., Weis, P., 2002. The Chiapas Massif (Mexico) revised: new geologic and isotopic data for basement characteristics. Neues Jahrbuch für Geologie und Paläontologie-Abhandlungen 225, 1–23.
Schmieder, M., Kring, DA, IODP-ICDP Expedition 364 Science Party 2017. Petrology of target dolerite in the Chicxulub Peak Ring and a possible source of K/Pg boundary Picotite Spinel, 48th Lunar and Planetary Science Conference. Abstract#1235.
Schmieder, M., Kring, D., Lapen, T., Gulick, S., Stockli, D., Rasmussen, C., Rae, A., Ferrière, L., Poelchau, M., Xiao, L., Wittmann A., and the IODP-ICDP Expedition 364 Science Party, 2017a. Sphene and TiO2 Assemblages in the Chicxulub Peak Ring: U-Pb Systematics and Implications for Shock Pressures, Temperatures, and Crater Cooling, 80th Annual Meeting of the Meteoritical Society 2017. Abstract # 6134.
Schmieder, M., Shaulis, B.J., Lapen, T.J., Kring, D.A., 2017b. U–Th–Pb systematics in zircon and apatite from the Chicxulub impact crater, Yucatán, Mexico. Geological Magazine.
Schmieder M, E.T.M., Kring D A. and the IODP–ICDP Expedition 364 Science Party, 2019. Microstructural Characterization of TiO2-II in the Chicxulub Peak Ring, 50th Lunar & Planetary Science Conference. Abstract#1658.
Seton, M., Müller, R.D., Zahirovic, S., Gaina, C., Torsvik, T., Shephard, G., Talsma, A., Gurnis, M., Turner, M., Maus, S., Chandler, M., 2012. Global continental and ocean basin reconstructions since 200Ma. Earth Sci. Rev. 113, 212–270.
Severs, M.J., Beard, J.S., Fedele, L., Hanchar, J.M., Mutchler, S.R., Bodnar, R.J., 2009. Partitioning behavior of trace elements between dacitic melt and plagioclase, orthopyroxene, and clinopyroxene based on laser ablation ICPMS analysis of silicate melt inclusions. Geochim. Cosmochim. Acta 73, 2123–2141.
Shaulis, B.J., Lapen, T.J., Casey, J.F., Reid, D.R., 2012. Timing and rates of flysch sedimentation in the Stanley Group, Ouachita Mountains, Oklahoma and Arkansas, U.S.A.: constraints from U-Pb Zircon ages of subaqueous Ash-Flow Tuffs. J. Sediment. Res. 82, 833–840.
Shaw, D.M., Dostal, J., Keays, R.R., 1976. Additional estimates of continental surface Precambrian shield composition in Canada. Geochim. Cosmochim. Acta 40, 73–83.
Simon-Labric, T., Brocard, G.Y., Teyssier, C., van der Beek, P.A., Fellin, M.G., Reiners, P.W., Authemayou, C., 2013. Preservation of contrasting geothermal gradients across the Caribbean-North America plate boundary (Motagua Fault, Guatemala). Tectonics 32, 993–1010.
Speer, J.A., Hoff, K.W., 1997. Elemental composition of the Alleghanian granitoid plutons of the southern Appalachians. In: Whalen, J.B., Hogan, J.P. (Eds.), Sinha, A.K. The Nature of Magmatism in the Appalachian Orogen, Geological Society of America, pp. 287–308.
Speer, J.A., Jr, H.Y.M., Gates, A.E., 1994. Generation, segregation, ascent, and emplacement of Alleghanian Plutons in the Southern Appalachians. The Journal of Geology 102, 249–267.
Steiner, M.B., Walker, J.D., 1996. Late Silurian plutons in Yucatan. Journal of Geophysical Research Solid Earth 101, 17727–17735.
Sun, S.S., McDonough, W.F., 1989. Chemical and isotopic systematics of oceanic basalts: implications for mantle composition and processes. Geological Society London Special Publications 42, 313–345.
Sylvester, P.J., 1998. Post-collisional strongly peraluminous granites. Lithos 45, 29–44.
Tanaka, T., Togashi, S., Kamioka, H., Amakawa, H., Kagami, H., Hamamoto, T., Yuhara, M., Orihashi, Y., Yoneda, S., Shimizu, H., Kunimaru, T., Takahashi, K., Yanagi, T., Nakano, T., Fujimaki, H., Shinjo, R., Asahara, Y., Tanimizu, M., Dragusanu, C., 2000. JNdi-1: a neodymium isotopic reference in consistency with LaJolla neodymium. Chem. Geol. 168, 279–281.
Terashima, S., Taniguchi, M., Mikoshiba, M., Imai, N., 1998. Preparation of two new GSJ geochemical reference materials: basalt JB-1b and coal fly ash JCFA-1. Geostand. Newslett. 22, 113–117.
Thirlwall, M.F., 1991. Long-term reproducibility of multicollector Sr and Nd isotope ratio analysis. Chemical Geology: Isotope Geoscience Section 94, 85–104.
Thorkelson, D.J., Breitsprecher, K., 2005. Partial melting of slab window margins: genesis of adakitic and non-adakitic magmas. Lithos 79, 25–41.
Torres, R., Ruiz, J., Jonathan Patchett, P., Manuel Grajales, J., 1999. Permo-Triassic Continental Arc in Eastern Mexico: Tectonic Implications for Reconstructions of Southern North America. pp. 191–196.
Vervoort, J.D., Blichert-Toft, J., 1999. Evolution of the depleted mantle: Hf isotope evidence from juvenile rocks through time. Geochim. Cosmochim. Acta 63, 533–556.
Vervoort, J.D., Patchett, P.J., Albarède, F., Blichert-Toft, J., Rudnick, R., Downes, H., 2000. Hf–Nd isotopic evolution of the lower crust. Earth Planet. Sci. Lett. 181, 115–129.
Wang, Q., Jifeng, X.U., Jian, P., Bao, Z., Zhao, Z., Chaofeng, L.I., Xiong, X., Jinlong, M.A., 2006. Petrogenesis of Adakitic porphyries in an extensional tectonic setting, Dexing, South China: implications for the Genesis of porphyry copper mineralization. J. Petrol. 47, 119–144.
Wang, Q., Wyman, D.A., Xu, J., Jian, P., Zhao, Z., Li, C., Xu, W., Ma, J., He, B., 2007a. Early Cretaceous adakitic granites in the Northern Dabie Complex, central China: implications for partial melting and delamination of thickened lower crust. Geochim. Cosmochim. Acta 71, 2609–2636.
Wang, Q., Wyman, D.A., Zhao, Z.H., Xu, J.F., Bai, Z.H., Xiong, X.L., Dai, T.M., Li, C.F., Chu, Z.Y., 2007b. Petrogenesis of Carboniferous adakites and Nb-enriched arc basalts in the Alataw area, northern Tianshan Range (western China): Implications for Phanerozoic crustal growth in the Central Asia orogenic belt. Chem. Geol. 236, 42–64.
Weber, B., Hecht, L., 2003. Petrology and geochemistry of metaigneous rocks from a Grenvillian basement fragment in the Maya block: the Guichicovi complex, Oaxaca, southern Mexico. Precambrian Res. 124, 41–67.
Weber, B., Köhler, H., 1999. Sm–Nd, Rb–Sr and U–Pb geochronology of a Grenville Terrane in Southern Mexico: origin and geologic history of the Guichicovi Complex. Precambrian Res. 96, 245–262.
Weber, B., Valencia, V.A., Schaaf, P., Pompa-Mera, V., Ruiz, J., 2008. Significance of provenance ages from the Chiapas Massif Complex (Southeastern Mexico): redefining the Paleozoic basement of the Maya Block and its evolution in a Peri-Gondwanan realm. J. Geol. 116, 619–639.
Weber, B., Scherer, E.E., Martens, U.K., Mezger, K., 2012. Where did the lower Paleozoic rocks of Yucatan come from? A U–Pb, Lu–Hf, and Sm–Nd isotope study. Chemical Geology s 312–313, 1–17.
Wiedenbeck, M., Alle, P., Corfu, F., Griffin, W.L., Meier, M., Oberli, F., Quadt, A.V., Roddick, J.C., Spiegel, W., 1995. Three Natural Zircon Standards for U-Th-Pb, Lu-Hf. Trace Element and REE Analyses. Geostandards Newsletter 19, 1–23.
Winchester, C., 2013. Alleghanian Plutonism in the Eastern Blue Ridge Province of the Southern Appalachians: Origin and Tectonic Setting. University of North Carolina, pp. 1–45.
Wittmann, A., van Soest, M., Hodges, K.V., Darling, J.R., Morgan, J.V., Gulick, S.P.S., Stockli, D., Rasmussen, C., Kring, D.A., Schmieder, M., 2018. Petrology and radioisotopic ages of allanite in the peak ring of the Chicxulub impact crater. Annual Meeting of the Meteoritical Society 81.
Wortel, M., Spakman, W., 1992. Structure and dynamics of subducted lithosphere in the Mediterranean region. Proceedings of the Koninklijke Nederlandse Akademie van Wetenschappen 95 (3), 325–347.
Xia, L.Q., Xu, X.Y., Xia, Z.C., Li, X.M., Ma, Z.P., Wang, L.S., 2004. Petrogenesis of Carboniferous rift-related volcanic rocks in the Tianshan, northwestern China. Geol. Soc. Am. Bull. 116, 419–433.
Xiao, L., Clemens, J.D., 2007. Origin of potassic (C-type) adakite magmas: experimental and field constraints. Lithos 95, 399–414.
Xiao, L., Zhang, H.F., Clemens, J.D., Wang, Q.W., Kan, Z.Z., Wang, K.M., Ni, P.Z., Liu, X.M., 2007. Late Triassic granitoids of the eastern margin of the Tibetan Plateau: geochronology, petrogenesis and implications for tectonic evolution. Lithos 96, 436–452.
Xiao, L., Zhao, J.W., Liu, H.S., Xiao, Z.Y., Morgan, J., Gulick, S., Kring, D., Claeys, P., Riller, U.a.t. E.S., 2017. Ages and Geochemistry of the Basement Granites of the Chicxulub Impact Crater: Implications for Peak Ring Formation, 48th Lunar and Planetary Science Conference. Abstract#1311.
Xiong, X.L., 2006. Trace element evidence for growth of early continental crust by melting of rutile-bearing hydrous eclogite. Geology 34, 945–948.
Xiong, X.L., Adam, J., Green, T.H., 2005. Rutile stability and rutile/melt HFSE partitioning during partial melting of hydrous basalt: implications for TTG genesis. Chem. Geol. 218, 339–359.

Yoshioka, S., Wortel, M., 1995. 3D numerical modeling of detachment of subducted lithosphere. 100(B10), 20223–20244.
Zartman, R.E., Doe, B.R., 1981. Plumbotectonics—the model. Tectonophysics 75, 135–162.
Zhang, L.Y., Ducea, M.N., Ding, L., Pullen, A., Kapp, P., Hoffman, D., 2014. Southern Tibetan Oligocene–Miocene adakites: a record of Indian slab tearing. Lithos 210–211, 209–223.
Zindler, A., Hart, S., 1986. Chemical Geodynamics. Annu. Rev. Earth Planet. Sci. 14, 493–571.
Zong, K., Klemd, R., Yuan, Y., He, Z., Guo, J., Shi, X., Liu, Y., Hu, Z., Zhang, Z., 2017. The assembly of Rodinia: the correlation of early Neoproterozoic (ca. 900Ma) high-grade metamorphism and continental arc formation in the southern Beishan Orogen, southern Central Asian Orogenic Belt (CAOB). Precambrian Res. 290, 32–48.